ACADÉMIE DES SCIENCES
INSTITUT DE FRANCE

*Comptes Rendus. Chimie*
Supplementary material to the article available at:
https://doi.org/10.5802/crchim.282

# Derivatives of trigonal lanthanide complexes by reaction with long aliphatic chain amines

**Yiwei Zhou [#,a], Christian Dirk Buch [#,a], Steen Hansgaard Hansen [a] and Stergios Piligkos [*,a]**

[a] Department of Chemistry, University of Copenhagen, Universitetsparken 5, DK-2100 Copenhagen Ø, Denmark

*E-mail:* piligkos@chem.ku.dk (S. Piligkos)

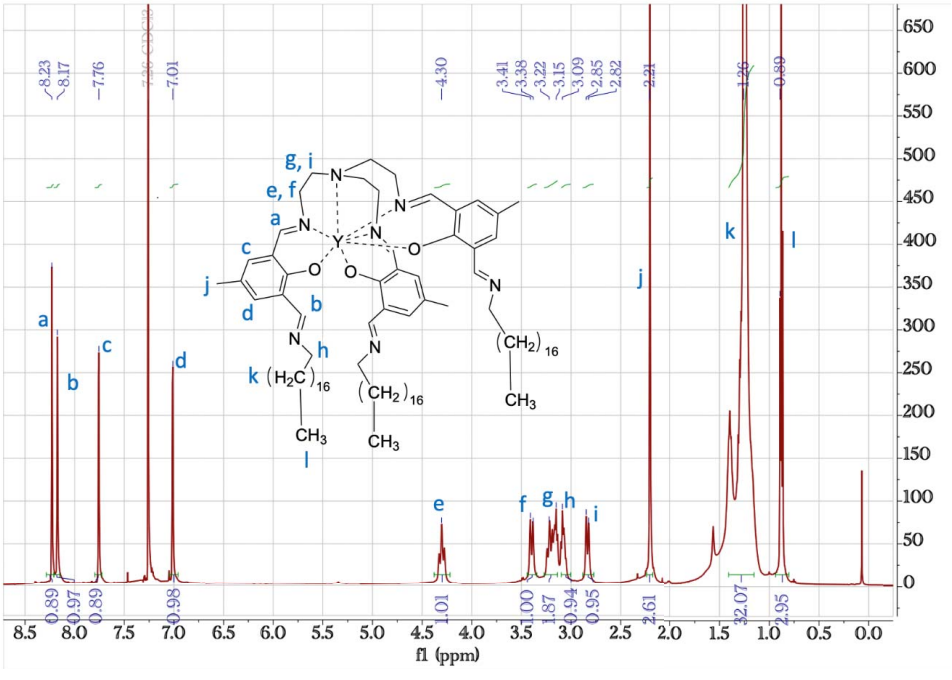


**Supplementary Figure S1.** $^1$H NMR of **YL$^{18}$** in $CDCl_3$, the peak at 1.5 ppm stems from water in the $CDCl_3$ and the signal at 7.26 stems from the deuterated solvent.

* Corresponding author.

# Contributed equally.

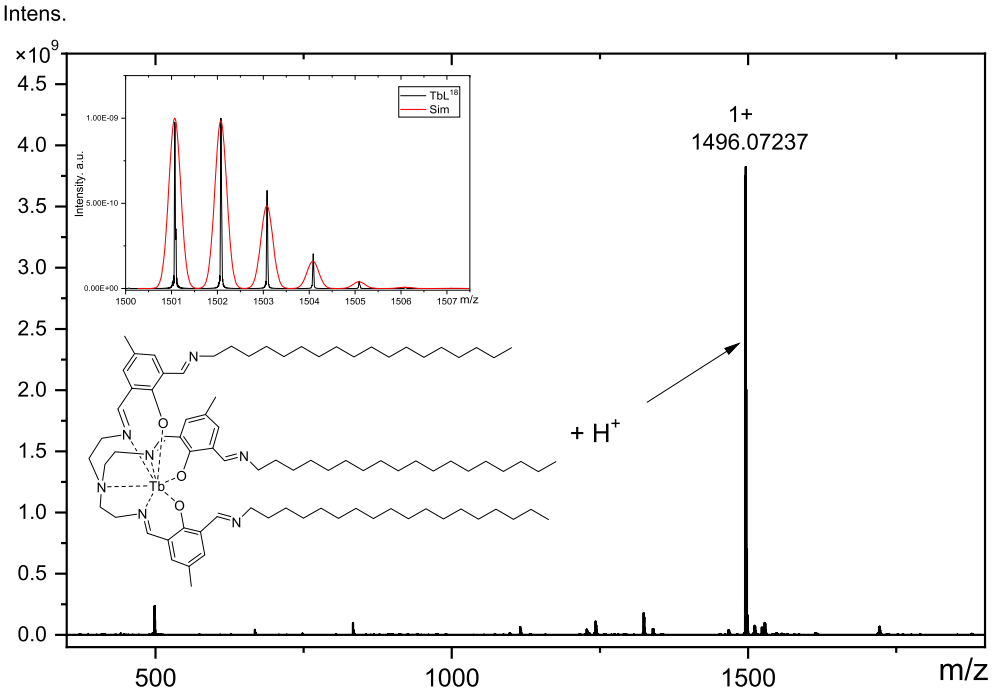


**Supplementary Figure S2.** Positive ion mode MALDI-MS of **TbL$^{18}$**. The simulated isotope distribution pattern and the detected signal from the molecular ion is shown in the insert.

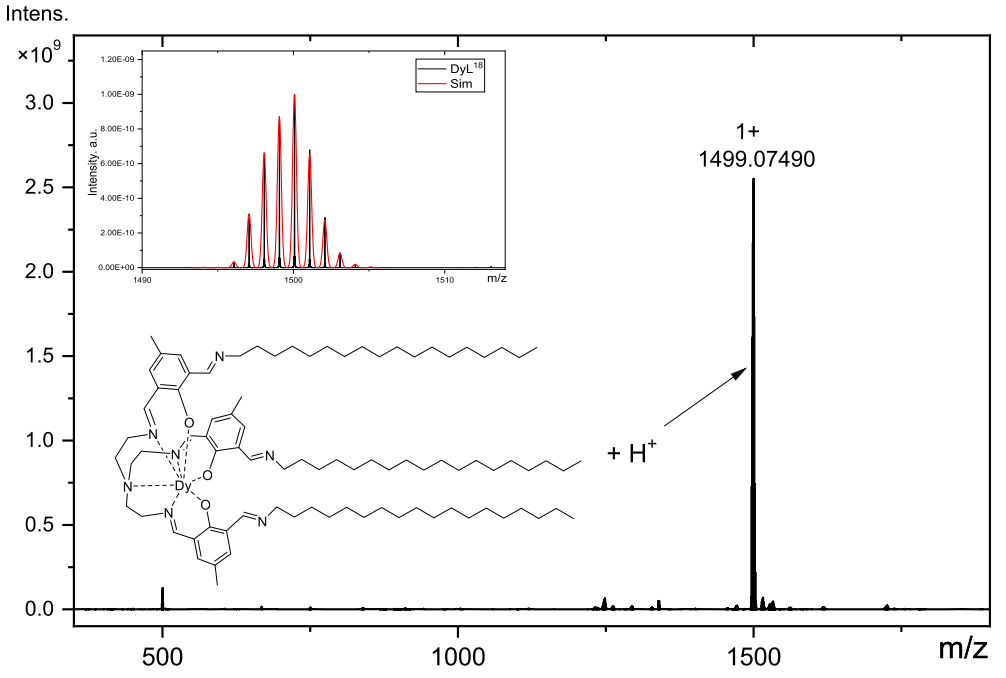


**Supplementary Figure S3.** Positive ion mode MALDI-MS of **DyL$^{18}$**. The simulated isotope distribution pattern and the detected signal from the molecular ion is shown in the insert.

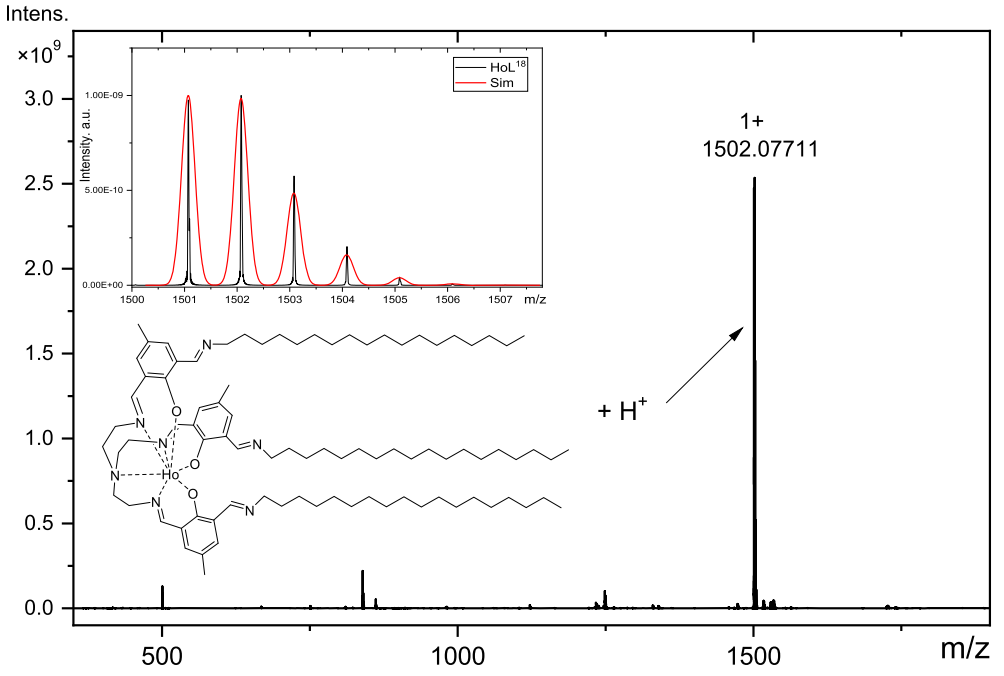


**Supplementary Figure S4.** Positive ion mode MALDI-MS of **HoL$^{18}$**. The simulated isotope distribution pattern and the detected signal from the molecular ion is shown in the insert.

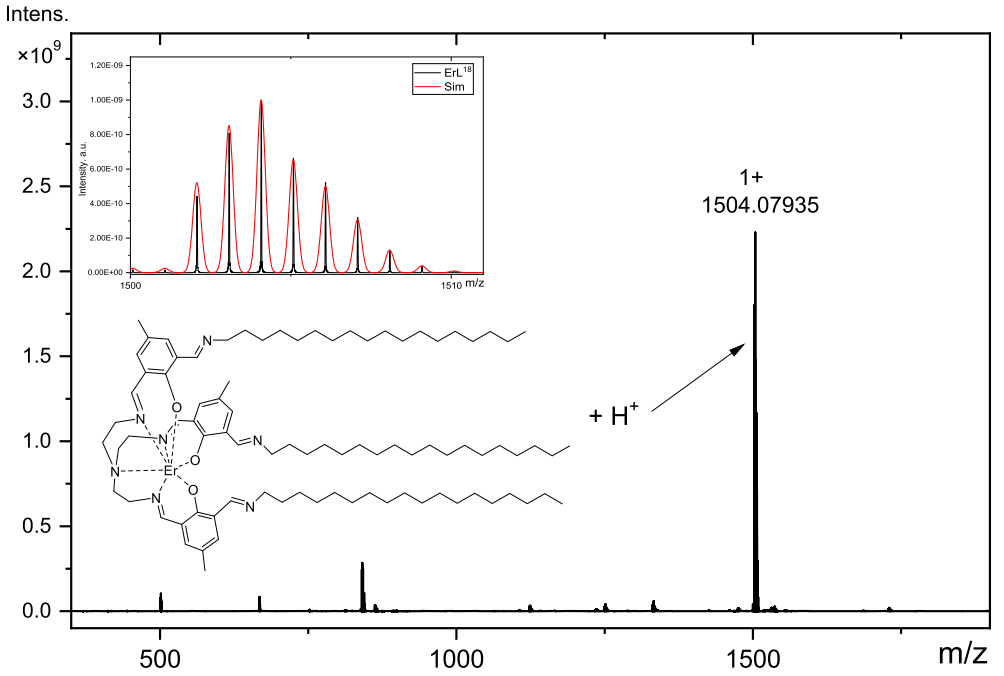


**Supplementary Figure S5.** Positive ion mode MALDI-MS of **ErL$^{18}$**. The simulated isotope distribution pattern and the detected signal from the molecular ion is shown in the insert.

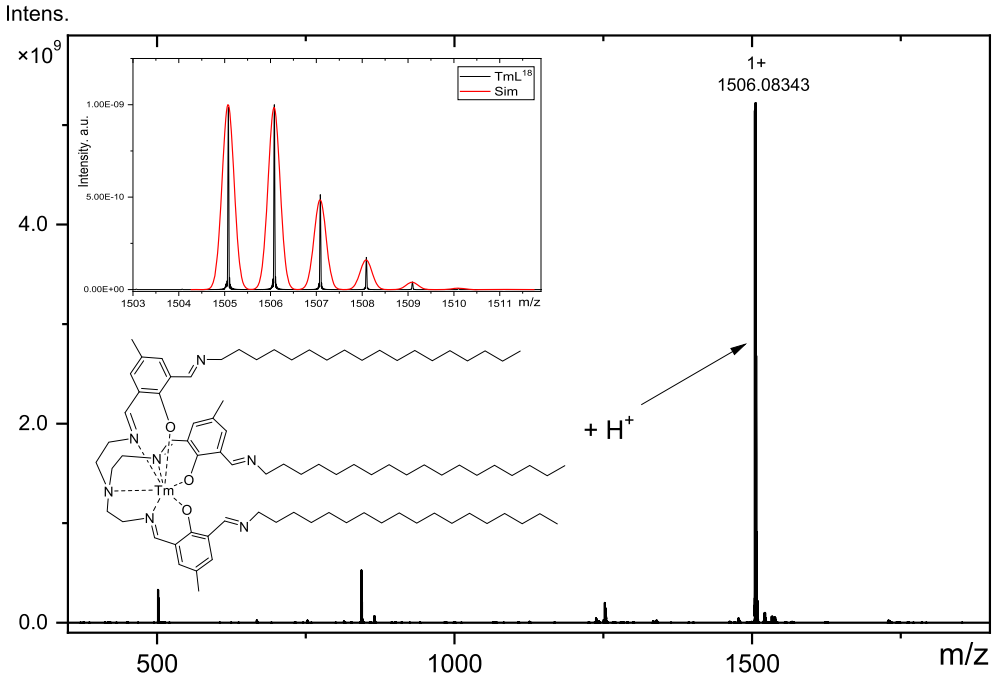


**Supplementary Figure S6.** Positive ion mode MALDI-MS of **TmL$^{18}$**. The simulated isotope distribution pattern and the detected signal from the molecular ion is shown in the insert.

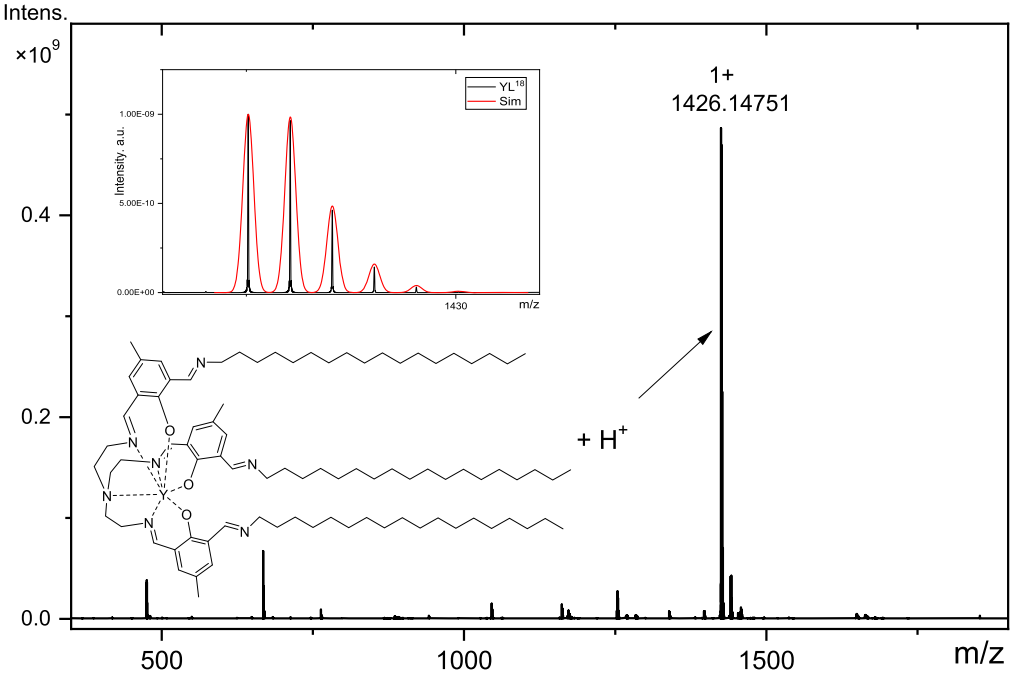


**Supplementary Figure S7.** Positive ion mode MALDI-MS of **YL$^{18}$**. The simulated isotope distribution pattern and the detected signal from the molecular ion is shown in the insert.

## 1. Infrared spectroscopy

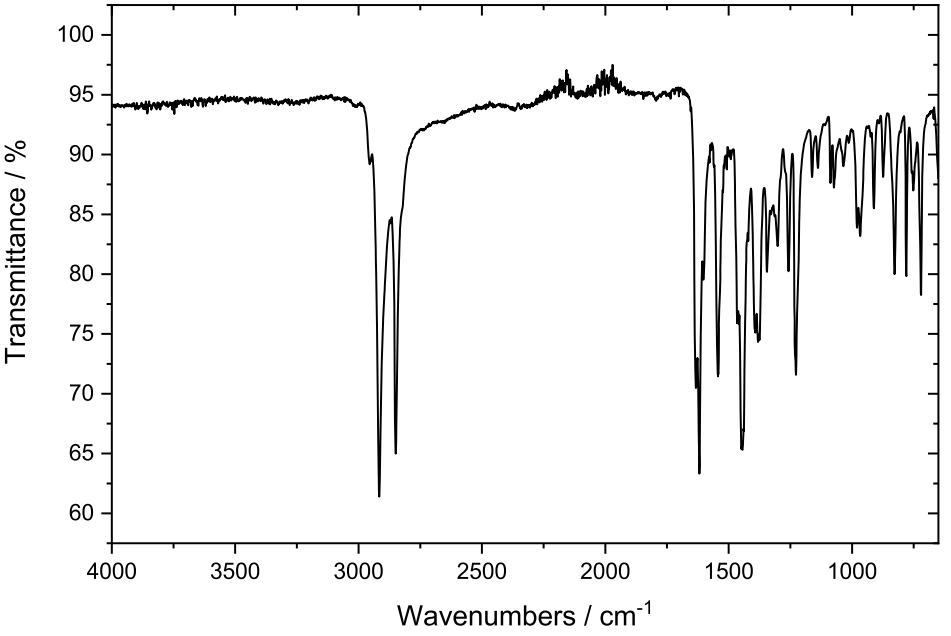


**Supplementary Figure S8.** IR spectrum of **TbL**[18].

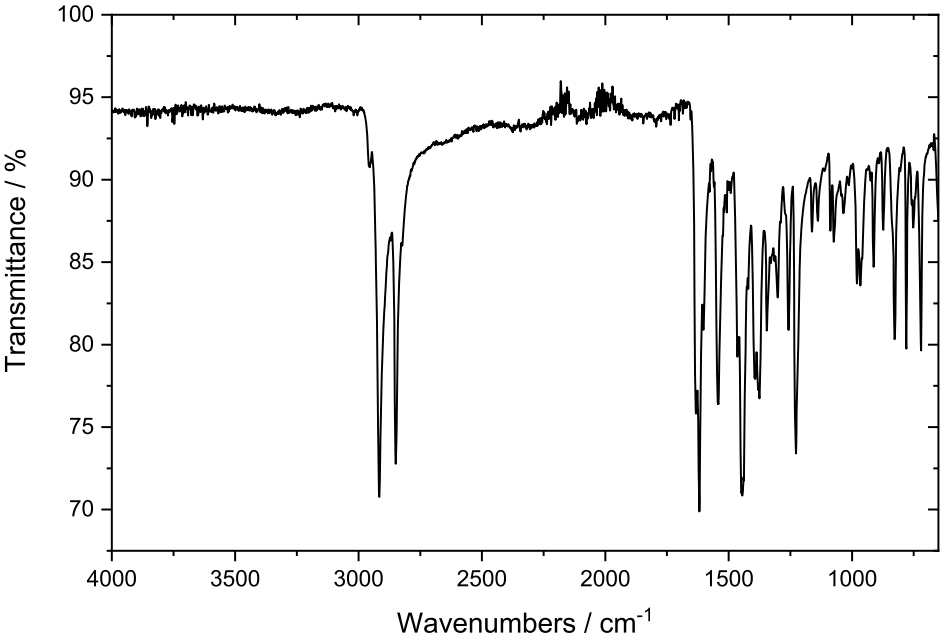


**Supplementary Figure S9.** IR spectrum of **DyL**[18].

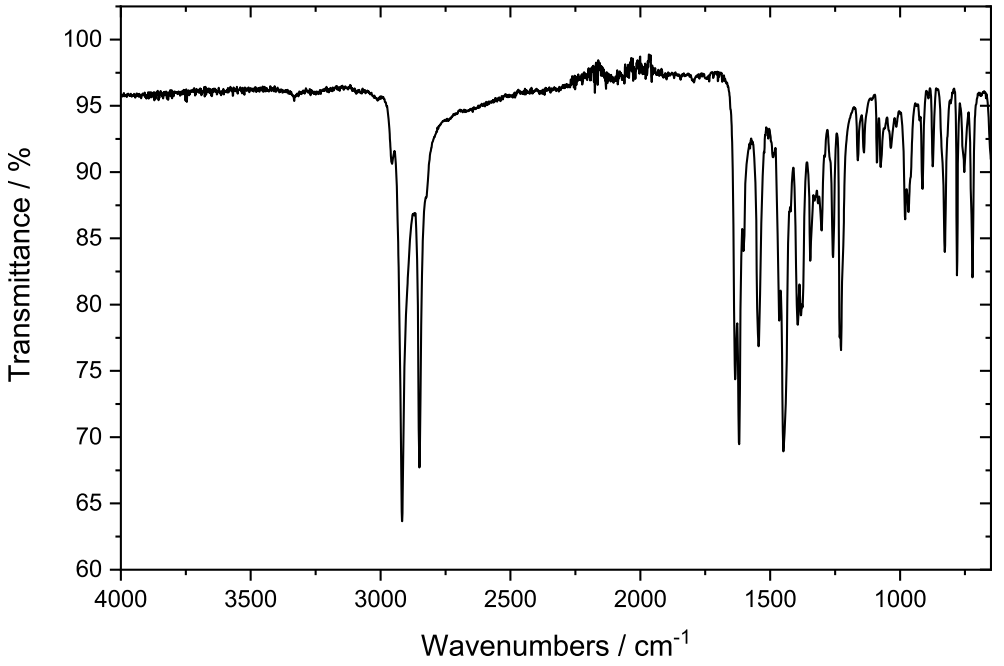


**Supplementary Figure S10.** IR spectrum of **HoL**[18].

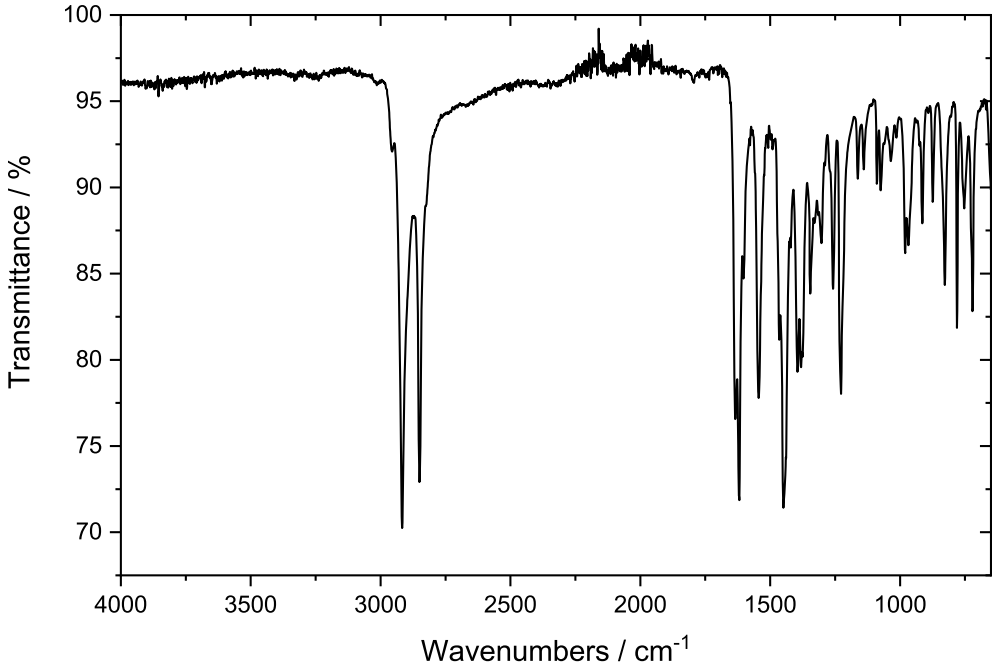


**Supplementary Figure S11.** IR spectrum of **ErL**[18].

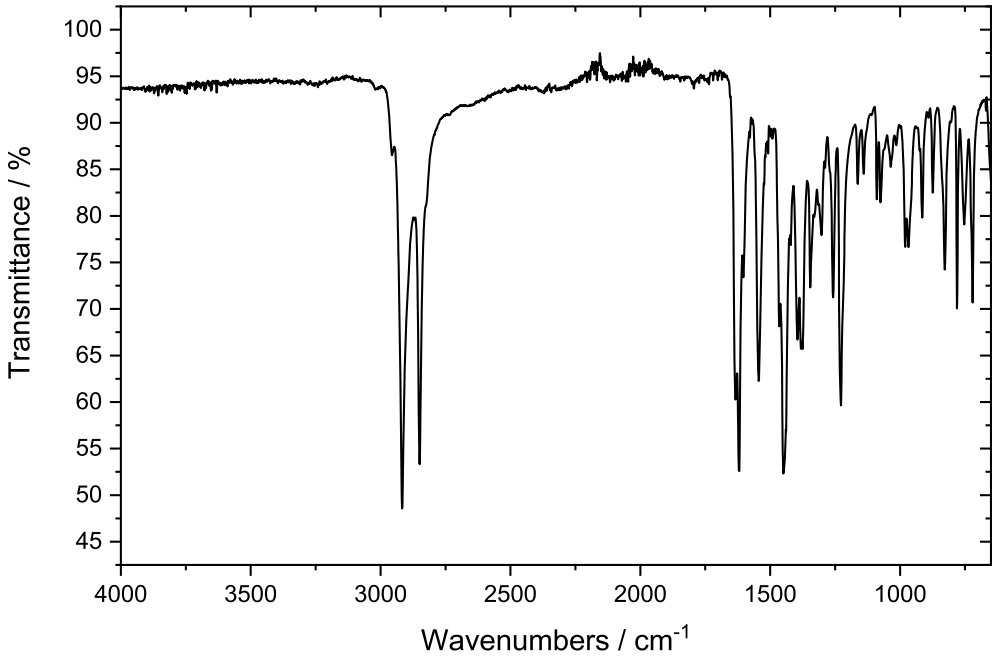


**Supplementary Figure S12.** IR spectrum of **TmL**[18].

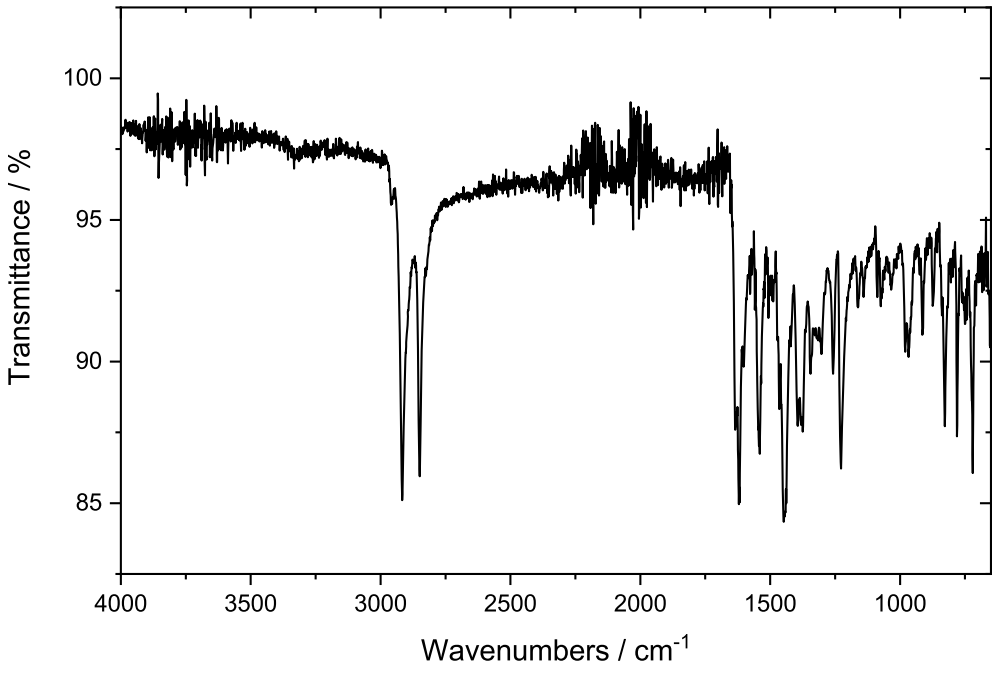


**Supplementary Figure S13.** IR spectrum of **YL**[18].

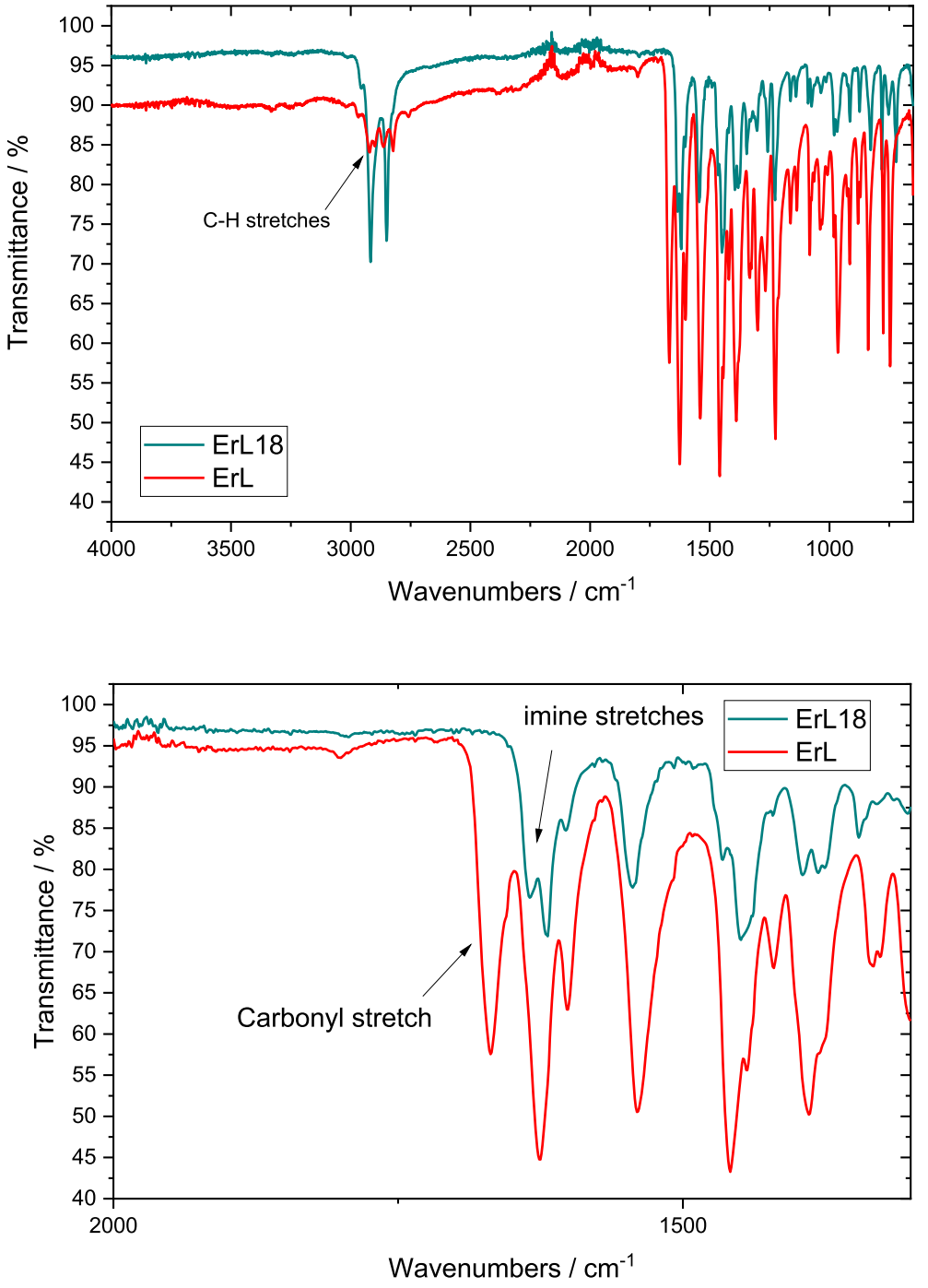


**Supplementary Figure S14.** Top: IR spectra of a polycrystalline powder of **ErL**$^{\mathbf{18}}$ (cyan) and of a polycrystalline powder of **ErL** (red). Bottom: Zoom in on the range 2000–1300 cm$^{-1}$ of the IR spectra of a polycrystalline powder of **ErL**$^{\mathbf{18}}$ (cyan) and of a polycrystalline powder of **ErL** (red).

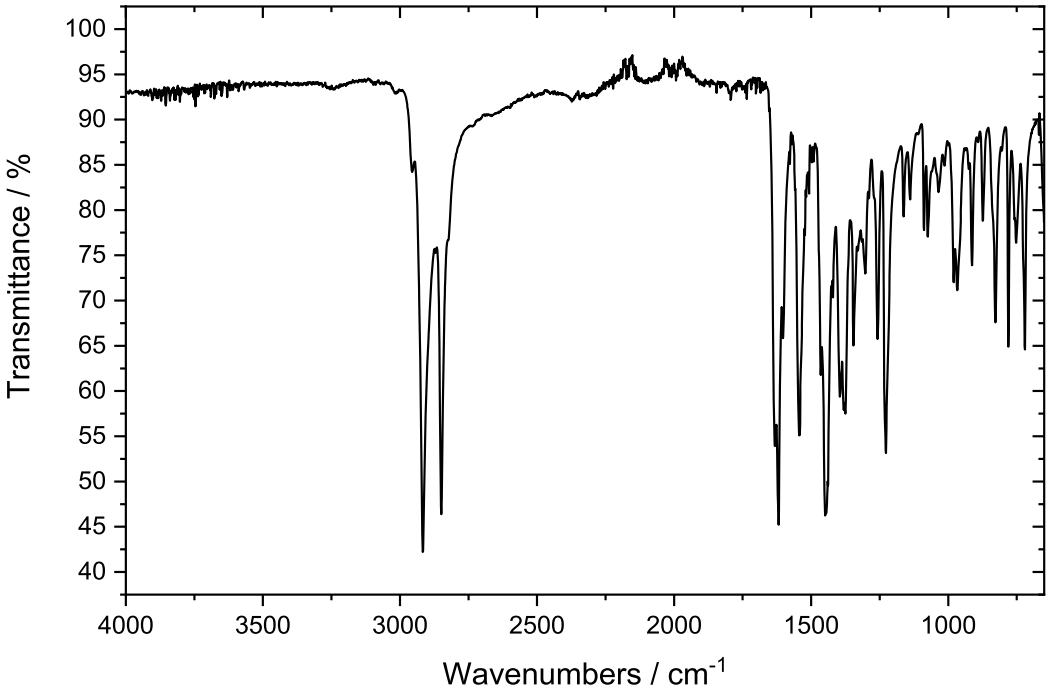


**Supplementary Figure S15.** IR spectrum of **Gd@YL$^{18}$** at 5% dilution.

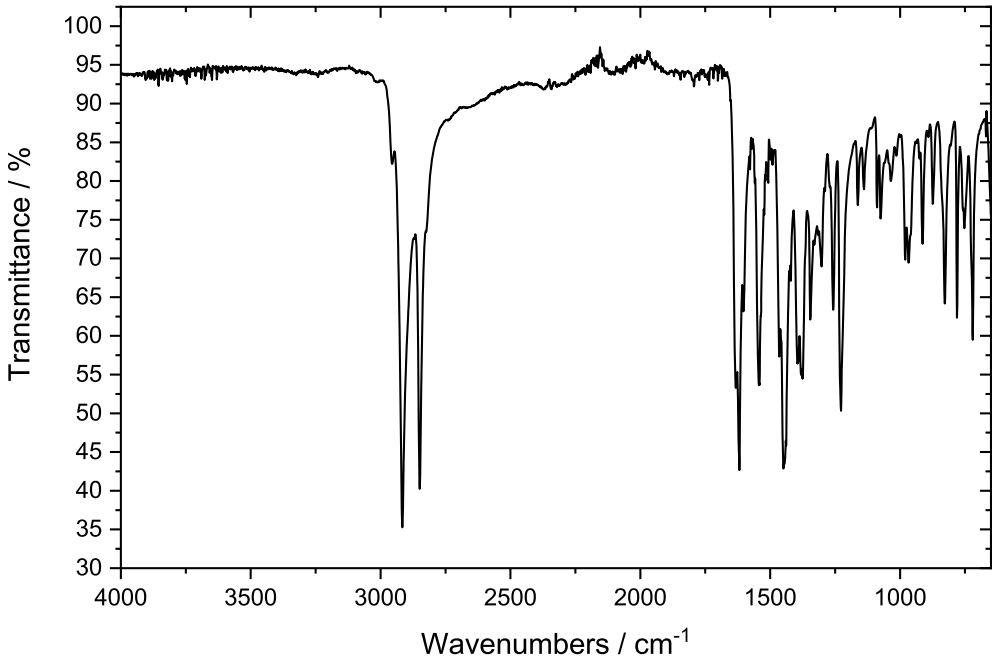


**Supplementary Figure S16.** IR spectrum of **Dy@YL$^{18}$** at 5% dilution.

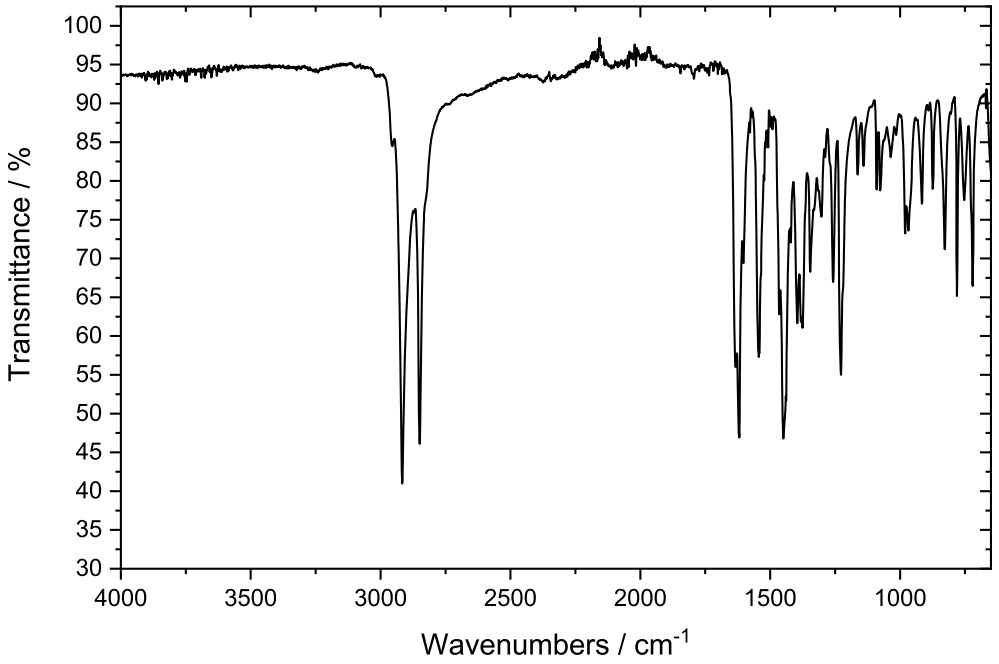


**Supplementary Figure S17.** IR spectrum of **Er@LuL$^{18}$** at 5% dilution.

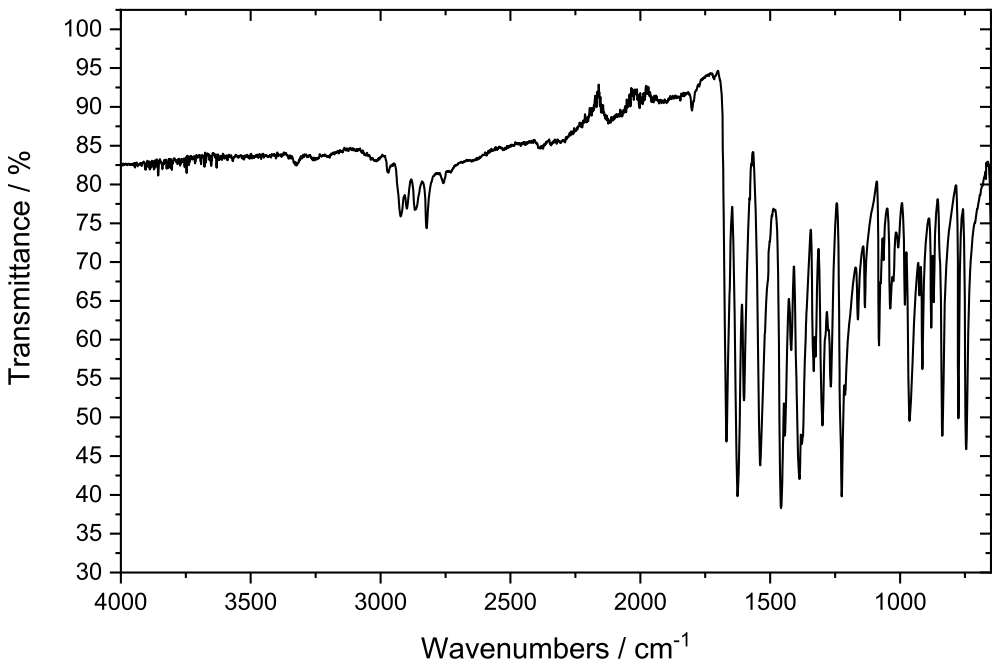


**Supplementary Figure S18.** IR spectrum of **Gd@YL** at 5% dilution.

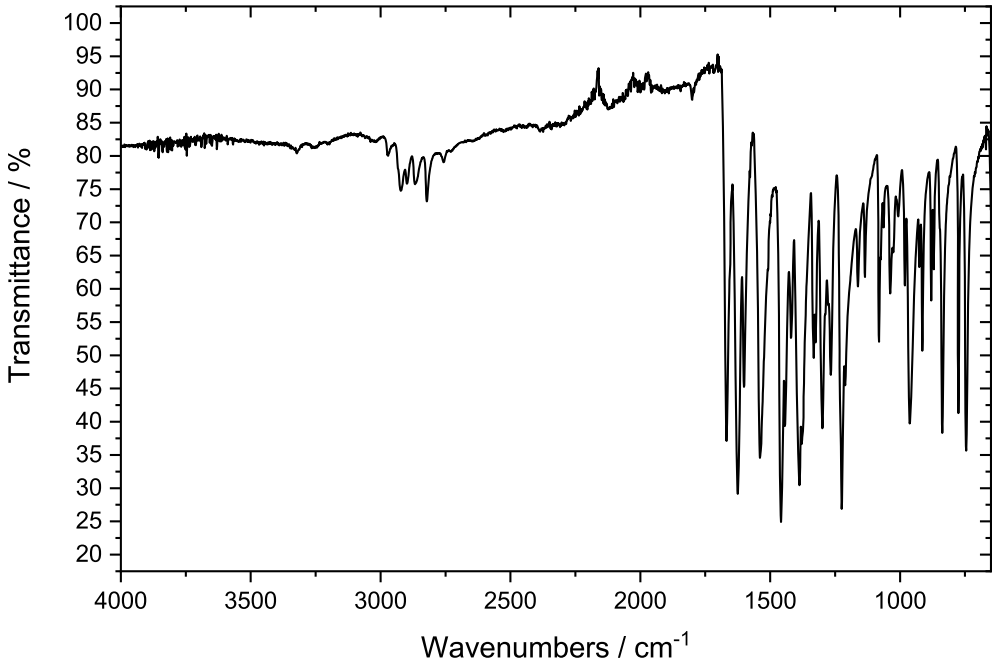


**Supplementary Figure S19.** IR spectrum of **Dy@YL** at 5% dilution.

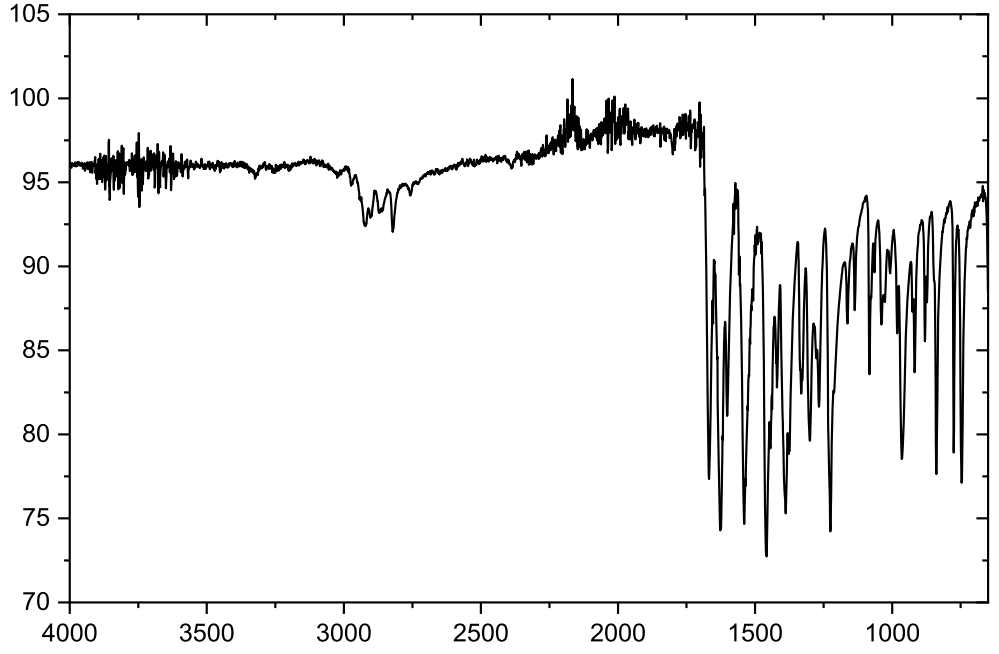


**Supplementary Figure S20.** IR spectrum of **Er@LuL** at 5% dilution.

## 2. Powder X-ray diffraction

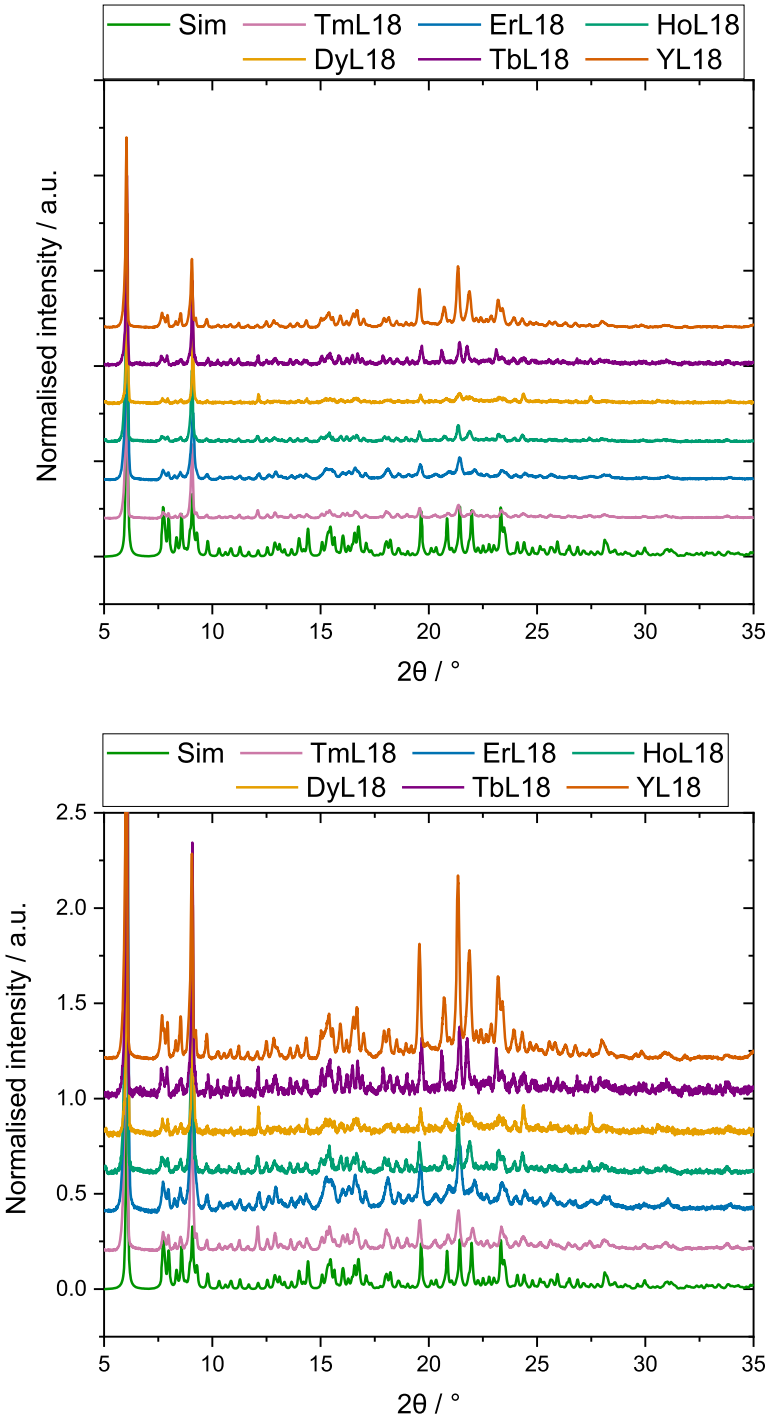


**Supplementary Figure S21.** PXRD data of **LnL**[18] (Ln = Tb–Tm, Y) (top), and PXRD data with the intensity multiplied by 3 (bottom). The simulated PXRD was calculated from a crystal structure measured at room temperature.

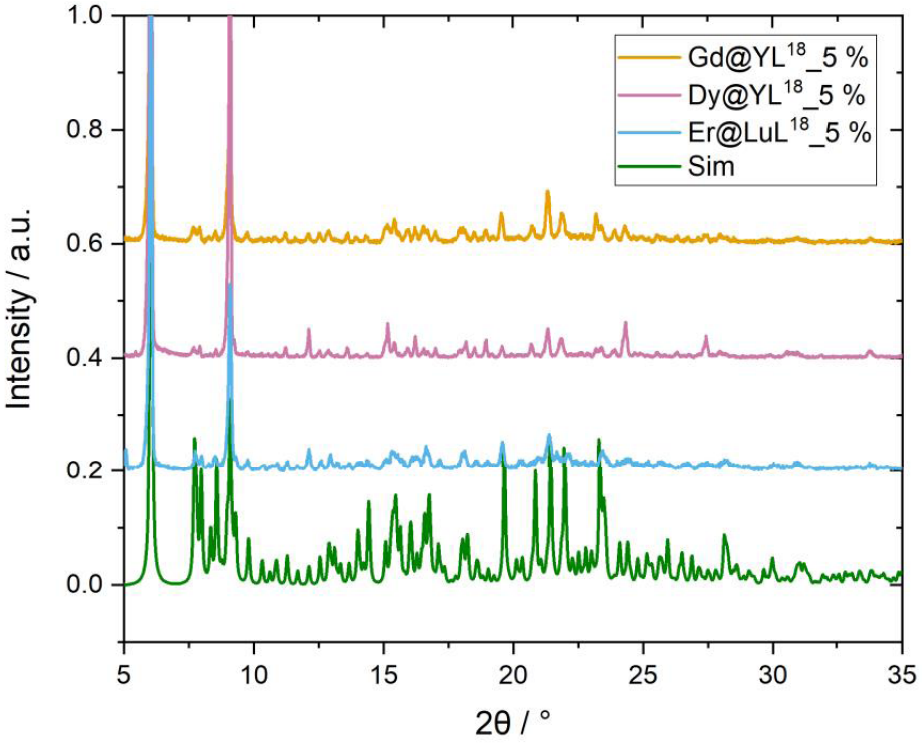


**Supplementary Figure S22.** PXRD of **Gd@YL[18]** at 5% dilution, **Dy@YL[18]** at 5% dilution, and **Er@LuL[18]** at 5 % dilution complexes. The simulated PXRD pattern was calculated from a crystal structure measured at room temperature.

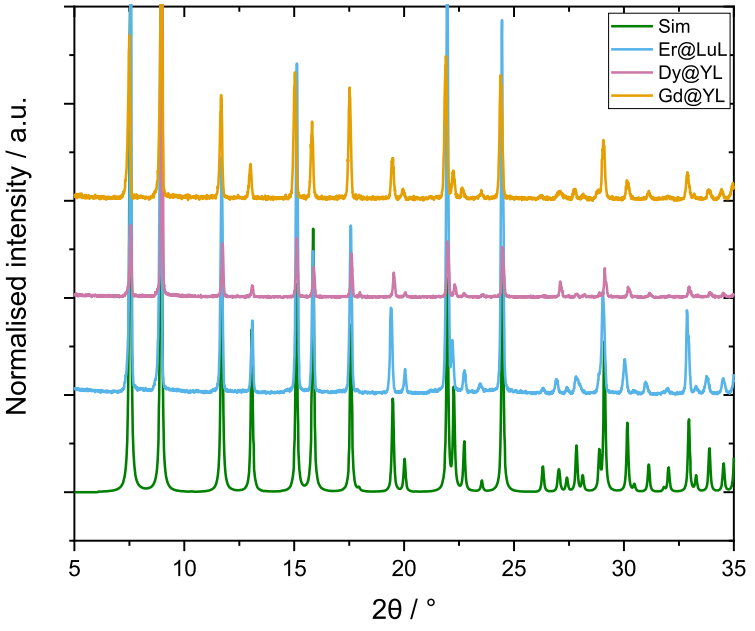


**Supplementary Figure S23.** PXRD data of diluted **Gd@YL** at 5% dilution, **Dy@YL** at 5% dilution, and **Er@LuL** at 5% dilution. The simulated PXRD pattern was calculated from a crystal structure measured at room temperature.

## 3. Crystallographic tables

**Supplementary Table S1.** Crystallographic data for **TbL$^{18}$**, **DyL$^{18}$** and **HoL$^{18}$**

| Complex | **TbL$^{18}$** | **DyL$^{18}$** | **HoL$^{18}$** |
|---|---|---|---|
| Empirical formula | $C_{87}H_{144}N_7O_3Tb$ | $C_{87}H_{144}DyN_7O_3$ | $C_{87}H_{144}HoN_7O_3$ |
| Formula weight | 1495.00 | 1498.58 | 1501.01 |
| Temperature/K | 100 | 100 | 100 |
| Crystal system | Triclinic | Triclinic | Triclinic |
| Space group | $P\bar{1}$ | $P\bar{1}$ | $P\bar{1}$ |
| $a$ (Å) | 12.4525(18) | 12.446(3) | 12.4376(12) |
| $b$ (Å) | 12.4793(18) | 12.503(3) | 12.4905(12) |
| $c$ (Å) | 30.021(5) | 29.997(8) | 30.010(3) |
| $\alpha$ (°) | 91.219(5) | 91.364(9) | 91.302(3) |
| $\beta$ (°) | 99.088(5) | 98.924(8) | 98.877(3) |
| $\gamma$ (°) | 115.649(5) | 115.685(8) | 115.817(3) |
| Volume (Å$^3$) | 4131.6(11) | 4134.0(18) | 4125.2(7) |
| Z | | 2 | |
| $\rho_{calc}$ g (cm$^3$) | 1.202 | 1.204 | 1.208 |
| $\mu$ (mm$^{-1}$) | 0.906 | 0.954 | 1.010 |
| F (000) | 1608.0 | 1610.0 | 1612.0 |
| Crystal size (mm$^3$) | 0.43 × 0.183 × 0.05 | 0.43 × 0.183 × 0.05 | 0.331 × 0.137 × 0.055 |
| $\lambda$ (MoK$\alpha$) | | 0.71073 | |
| 2$\Theta$ range for data collection (°) | 4.004 to 54.206 | 4.004 to 50.7 | 4.004 to 54.968 |
| Index ranges | $-15 \le h \le 15$, $-15 \le k \le 15$, $-38 \le l \le 38$ | $-14 \le h \le 14$, $-15 \le k \le 15$, $-36 \le l \le 36$ | $-16 \le h \le 16$, $-16 \le k \le 16$, $-38 \le l \le 38$ |
| Reflections collected | 158,077 | 136,453 | 147,625 |
| Independent reflections | 18168 [$R_{int} = 0.0728$, $R_{sigma} = 0.0392$] | 15,066 [$R_{int} = 0.0794$, $R_{sigma} = 0.0394$] | 18,886 [$R_{int} = 0.0720$, $R_{sigma} = 0.0427$] |
| Data/restraints/ parameters | 18,168/0/889 | 15,066/0/889 | 18,886/0/889 |
| Goodness-of-fit on $F^2$ | 1.053 | 1.043 | 1.066 |
| Final $R$ indexes [$I \ge 2\sigma(I)$] | $R_1 = 0.0287$, $\omega R_2 = 0.0600$ | $R_1 = 0.0278$, $\omega R_2 = 0.0536$ | $R_1 = 0.0339$, $wR_2 = 0.072$ |
| Final $R$ indexes [all data] | $R_1 = 0.0401$, $\omega R_2 = 0.0633$ | $R_1 = 0.0391$, $\omega R_2 = 0.0568$ | $R_1 = 0.0461$, $wR_2 = 0.0777$ |
| Largest diff. peak/hole/e (Å$^{-3}$) | 0.61/−0.78 | 0.55/−0.57 | 1.74/−1.29 |

## 4. Crystal structures

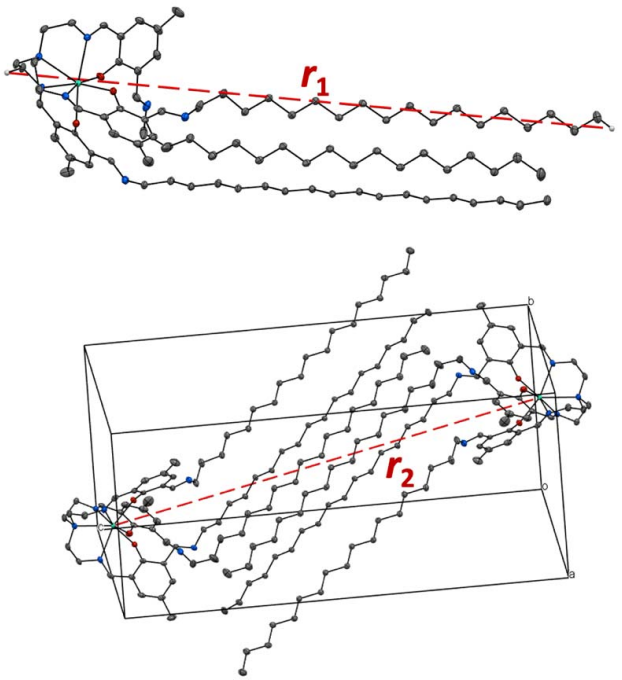


**Supplementary Figure S24.** Solid state structure (top) and unit cell (bottom) of **TbL$^{18}$**. The two distances $r_1$ and $r_2$ indicate the longest intramolecular distance in **TbL$^{18}$** and the longest distance between two Tb(III) centres in the unit cell, respectively. Colour code: Tb, green; N, blue; O, red; C, grey; H, white. All hydrogen atoms except for the ones defining the longest intramolecular distance have been omitted for clarity. Thermal ellipsoids are set to 50% probability.

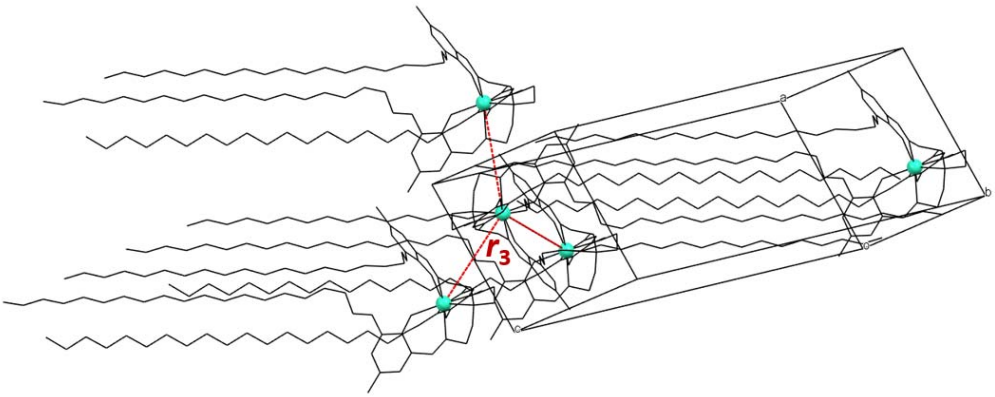


**Supplementary Figure S25.** Illustration of the three closest neighbouring complexes in **TbL$^{18}$**.

**Supplementary Table S2.** Comparisons of selected distances in **TbL**[18], **DyL**[18], **HoL**[18], **TbL**, **DyL** and **HoL**. The distances in **TbL**, **DyL** and **HoL** are obtained from literature [1]

| | Distance (Å) | | | |
|---|---|---|---|---|
| | $r_1$ | $r_2$ | $r_3$ | $r_4$ |
| | | | 7.899 | 12.479 |
| **TbL**[18] | 32.767 | 29.958 | 7.168 | 12.453 |
| | | | 6.999 | 12.352 |
| TbL | 13.228 | 7.780 | 7.780 | 13.448 |
| | | | 7.927 | 12.503 |
| **DyL**[18] | 32.799 | 29.996 | 7.170 | 12.503 |
| | | | 6.996 | 12.446 |
| DyL | 13.155 | 7.766 | 7.766 | 13.421 |
| | | | 7.897 | 13.244 |
| **HoL**[18] | 32.829 | 30.017 | 7.159 | 12.491 |
| | | | 7.002 | 12.438 |
| HoL | 13.112 | 7.761 | 7.761 | 13.411 |

Illustrations of the distances $r_1$, $r_2$, $r_3$, and $r_4$ are shown in Figures S24–S26 and S28–S31.

**Supplementary Table S3.** Comparison of selected bond lengths in **TbL**[18], **DyL**[18] and **HoL**[18]

| Bond length (Å) | Ln-O1A | Ln-O1B | Ln-O1C | Ln-N2A | Ln-N2B | Ln-N2C | Ln-N1 |
|---|---|---|---|---|---|---|---|
| **TbL**[18] | 2.1949(14) | 2.2034(14) | 2.2003(14) | 2.4787(17) | 2.4681(17) | 2.4763(18) | 2.6346(18) |
| **DyL**[18] | 2.1865(16) | 2.1905(14) | 2.1994(15) | 2.4613(18) | 2.462(2) | 2.4622(19) | 2.6314(19) |
| **HoL**[18] | 2.1790(16) | 2.1792(15) | 2.1923(15) | 2.4530(19) | 2.4532(2) | 2.454(2) | 2.631(2) |

**Supplementary Table S4.** Comparison of selected bond angles in **TbL**[18], **DyL**[18] and **HoL**[18]

| Bond angle (°) | ∠N2A-N2B-N2C | ∠N2B-N2A-N2C | ∠N2A-N2C-N2B | ∠N1-Ln-N2A | ∠N1-Ln-N2B | ∠N1-Ln-N2C | ∠N1-Ln-O1A | ∠N1-Ln-O1B | ∠N1-Ln-O1C | ∠O1A-O1B-O1C | ∠O1B-O1A-O1C | ∠O1A-O1C-O1B |
|---|---|---|---|---|---|---|---|---|---|---|---|---|
| **TbL**[18] | 61.30(4) | 61.44(4) | 57.26(4) | 68.69(6) | 69.05(6) | 69.03(6) | 126.65(6) | 124.32(5) | 127.09(5) | 60.27(4) | 60.51(4) | 59.22(4) |
| **DyL**[18] | 61.21(5) | 61.44(5) | 57.35(5) | 68.90(6) | 69.03(6) | 68.92(6) | 127.61(6) | 124.46(5) | 127.09(6) | 59.74(5) | 61.07(5) | 59.19(5) |
| **HoL**[18] | 61.11(5) | 61.41(5) | 57.49(5) | 69.11(7) | 69.09(7) | 68.93(6) | 127.67(7) | 124.65(6) | 127.13(6) | 59.92(5) | 61.01(5) | 59.08(5) |

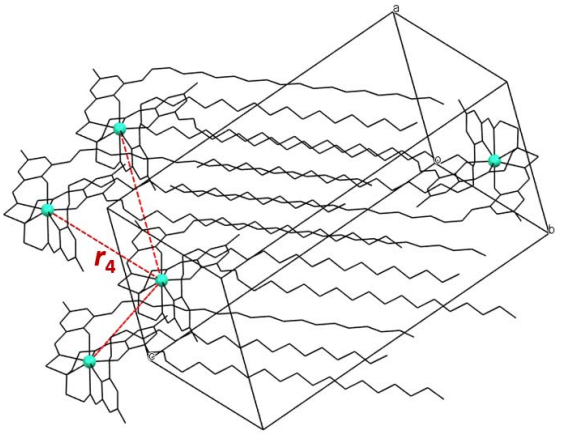


**Supplementary Figure S26.** The distance of the three closest neighbouring complexes with chains pointing in the same direction in **TbL**[18].

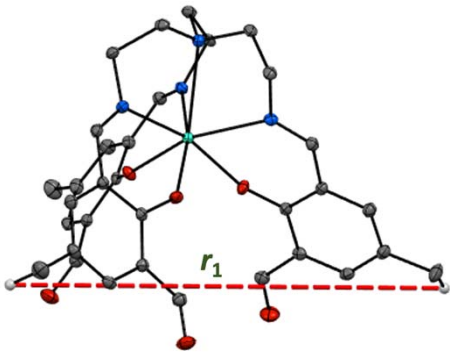


**Supplementary Figure S28.** Solid state structure of **TbL** showing the longest intra molecular distance, $r_1$. Hydrogen atoms have been omitted for clarity except for the hydrogens which are part of $r_1$. Colour code: Tb, cyan; N, blue; O, red; C, grey; H, white. Thermal ellipsoids are set to 50% probability.

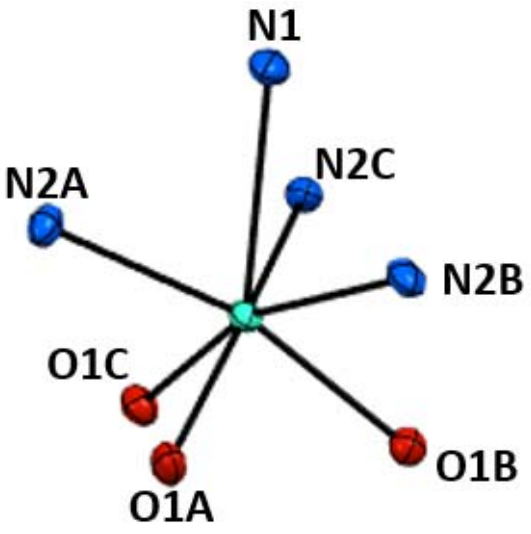


**Supplementary Figure S27.** The distorted monocapped octahedral coordination environment around Tb(III) in **TbL**[18]. Colour code: Tb, cyan; N, blue; O, red. Thermal ellipsoids are set to 50% probability.

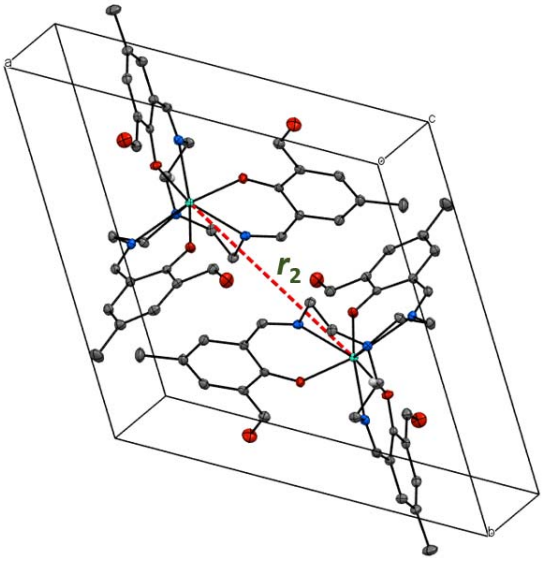


**Supplementary Figure S29.** Unit cell of **TbL** with $r_2$, the distance between two Tb(III) centres. Hydrogen atoms have been omitted for clarity. Colour code: Tb, cyan; N, blue; O, red; C, grey; H, white. Thermal ellipsoids are set to 50% probability.

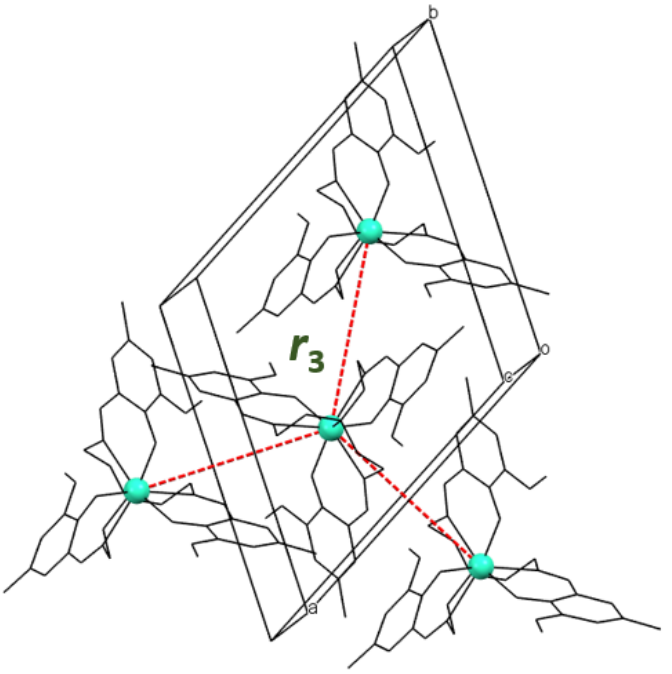


**Supplementary Figure S30.** Illustration of the three closest neighbouring complexes in **TbL**.

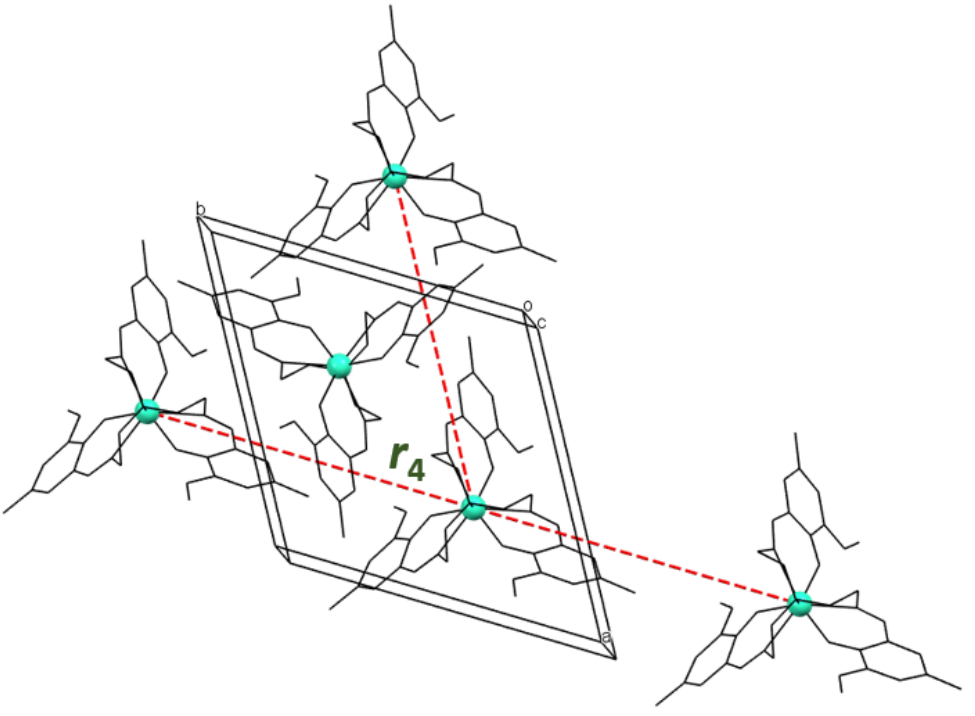


**Supplementary Figure S31.** The distance of the three closest neighbouring complexes with chains pointing in the same direction in **TbL**.

## 5. Variable-temperature-variable-field magnetisations

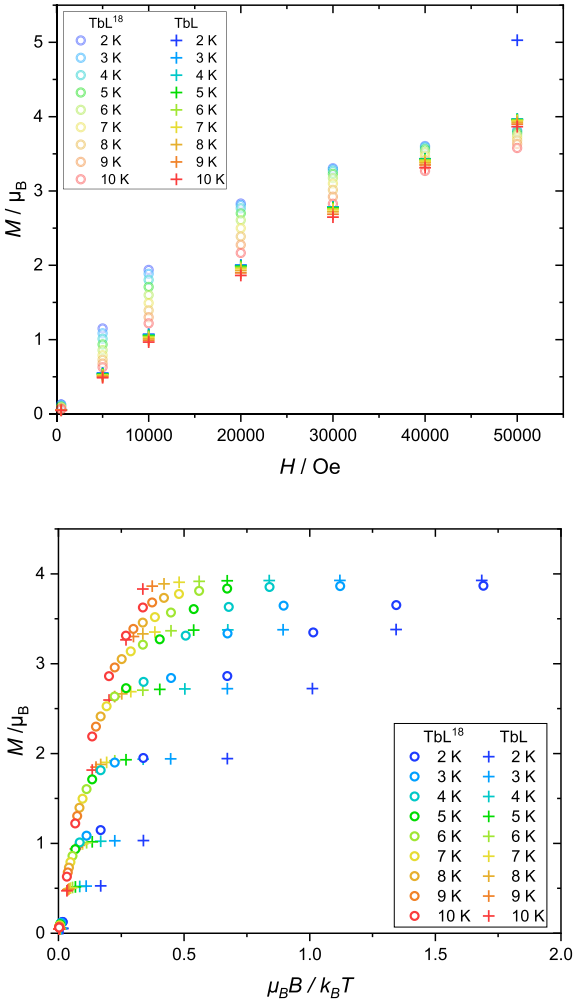


**Supplementary Figure S32.** Comparison of VTVB measurements (top) and reduced magnetisation (bottom) of **TbL$^{18}$** (circles) and **TbL** (crosses). The **TbL** values are obtained from literature [1].

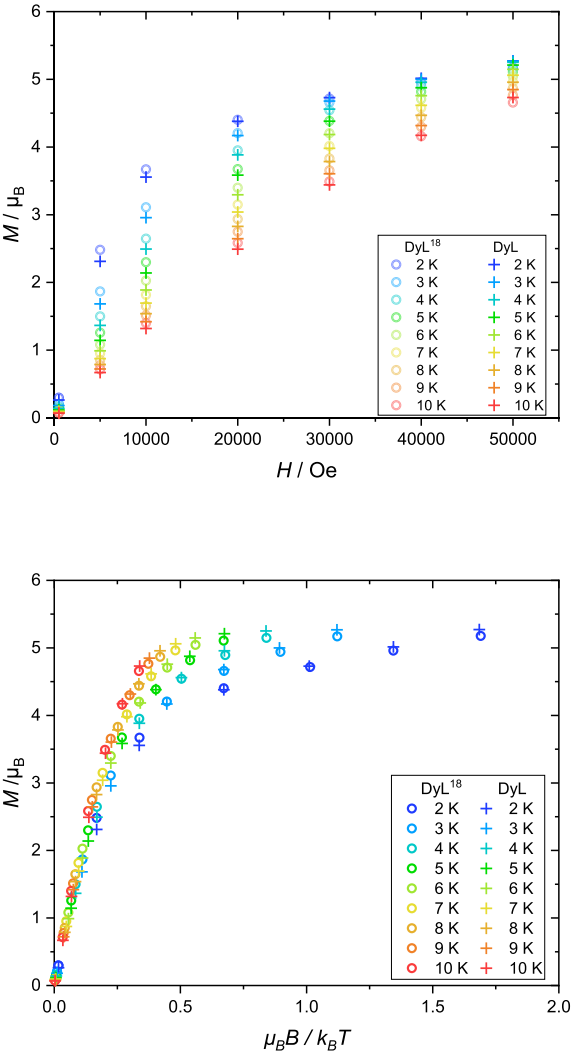


**Supplementary Figure S33.** Comparison of VTVB measurements (top) and reduced magnetisation (bottom) of **DyL$^{18}$** (circles) and **DyL** (crosses). The **DyL** values are obtained from literature [1].

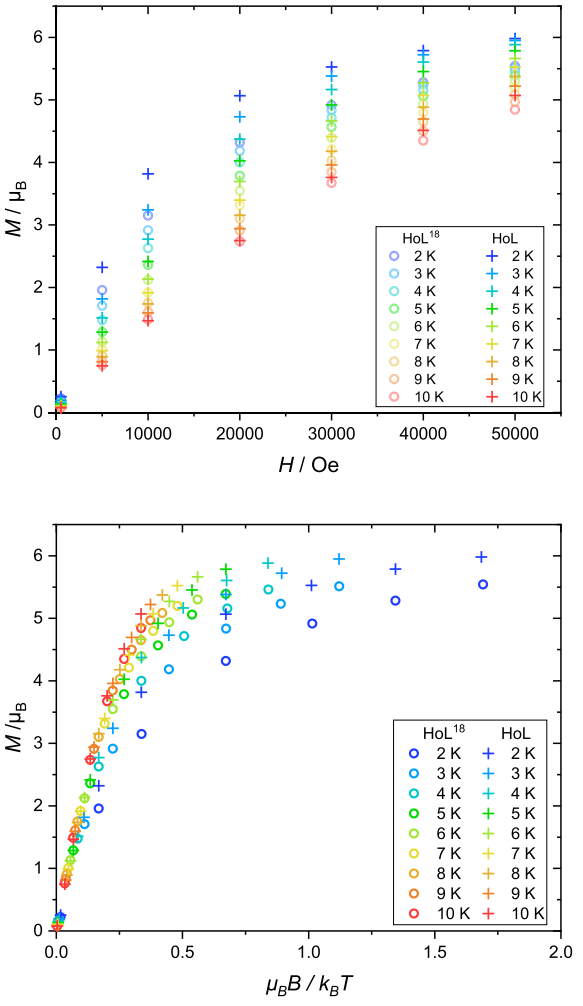


**Supplementary Figure S34.** Comparison of VTVB measurements (top) and reduced magnetisation (bottom) of **HoL$^{18}$** (circles) and **HoL** (crosses). The **HoL** values are obtained from literature.

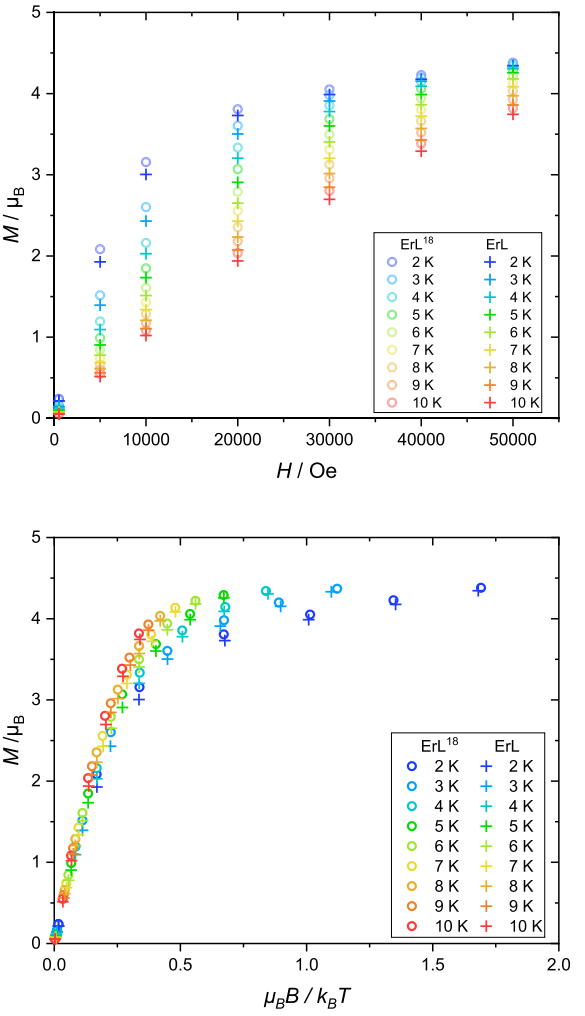


**Supplementary Figure S35.** Comparison of VTVB measurements (top) and reduced magnetisation (bottom) of **ErL$^{18}$** (circles) and **ErL** (crosses). The **ErL** values are obtained from literature [1].

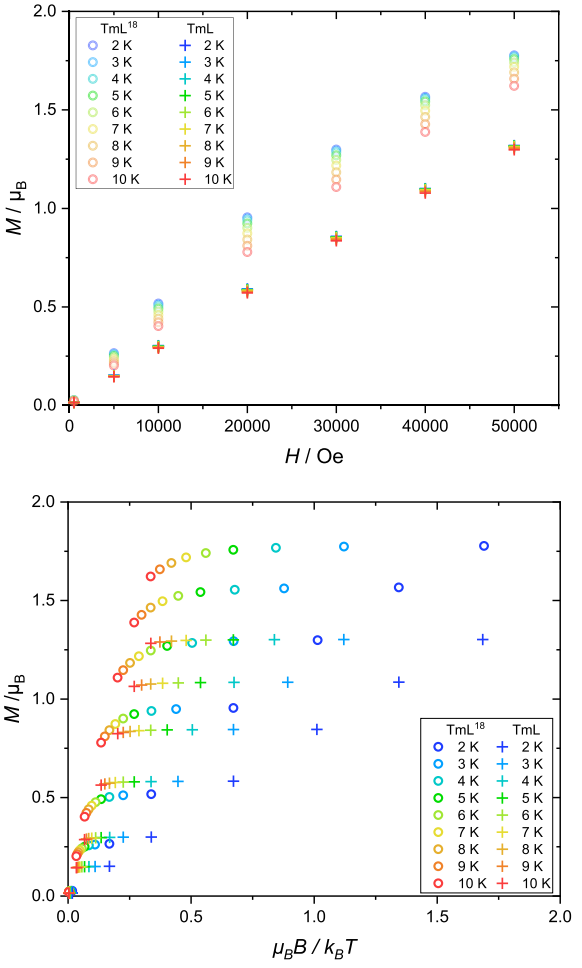


**Supplementary Figure S36.** Comparison of VTVB measurements (top) and reduced magnetisation (bottom) of **TmL**$^{18}$ (circles) and **TmL** (crosses). The **TmL** values are obtained from literature [1].

## 6. Ac susceptibility

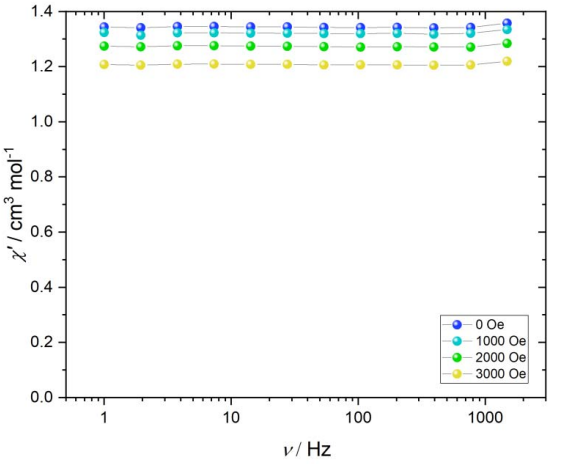


**Supplementary Figure S37.** Field dependence of the in-phase signal of the ac magnetic susceptibility of **TbL**$^{18}$. Solid lines are guidelines for the eye.

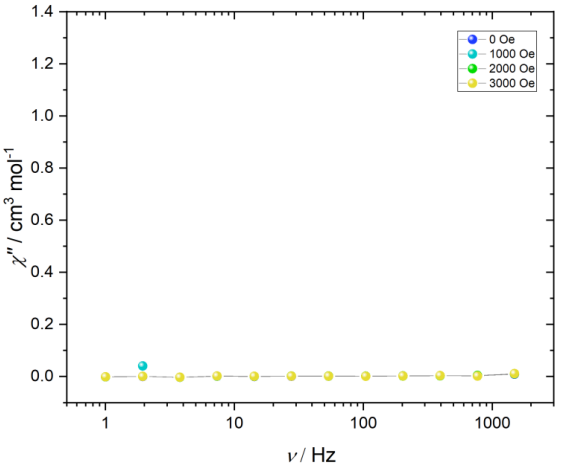


**Supplementary Figure S38.** Field dependence of the out-of-phase signal of the ac magnetic susceptibility of **TbL**$^{18}$. Solid lines are guidelines for the eye.

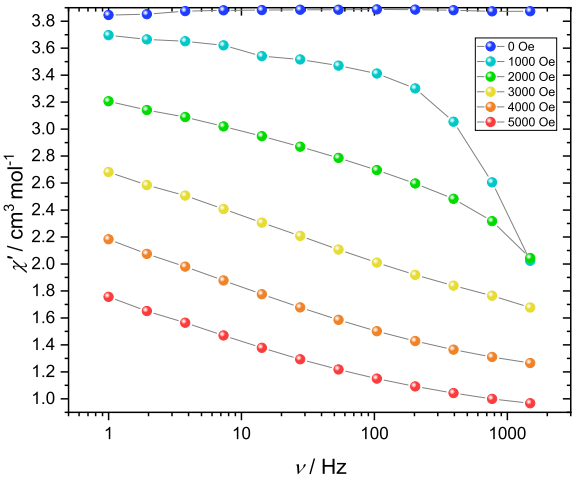


**Supplementary Figure S39.** Field dependence of the in-phase signal of the ac magnetic susceptibility of **DyL**[18]. Solid lines are guidelines for the eye.

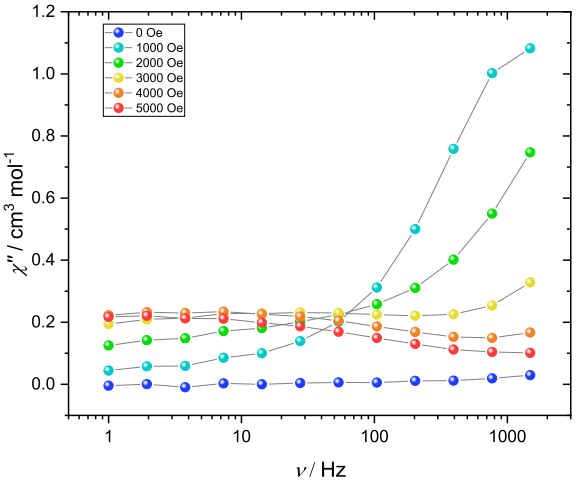


**Supplementary Figure S40.** Field dependence of the out-of-phase signal of the ac magnetic susceptibility of **DyL**[18]. Solid lines are guidelines for the eye.

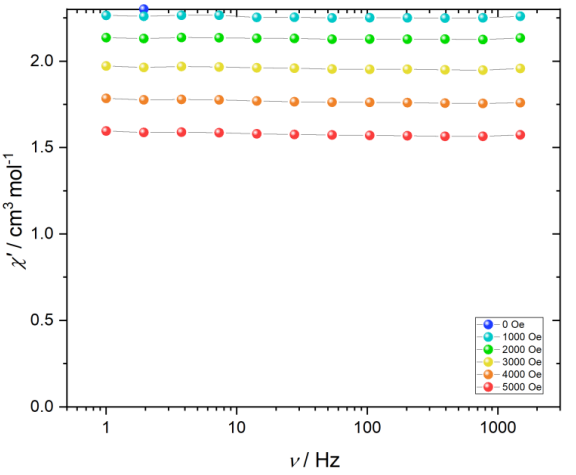


**Supplementary Figure S41.** Field dependence of the in-phase signal of the ac magnetic susceptibility of **HoL**[18]. Solid lines are guidelines for the eye.

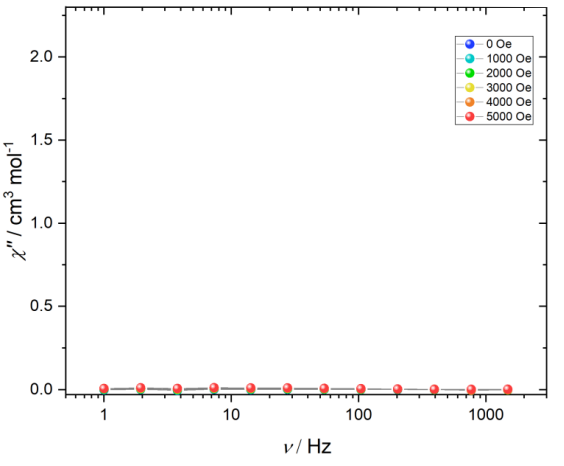


**Supplementary Figure S42.** Field dependence of the out-of-phase signal of the ac magnetic susceptibility of **HoL**[18]. Solid lines are guidelines for the eye.

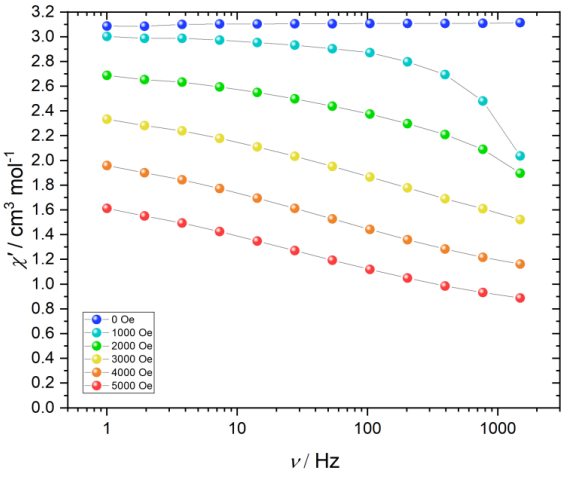


**Supplementary Figure S43.** Field dependence of the in-phase signal of the ac magnetic susceptibility of **ErL**[18]. Solid lines are guidelines for the eye.

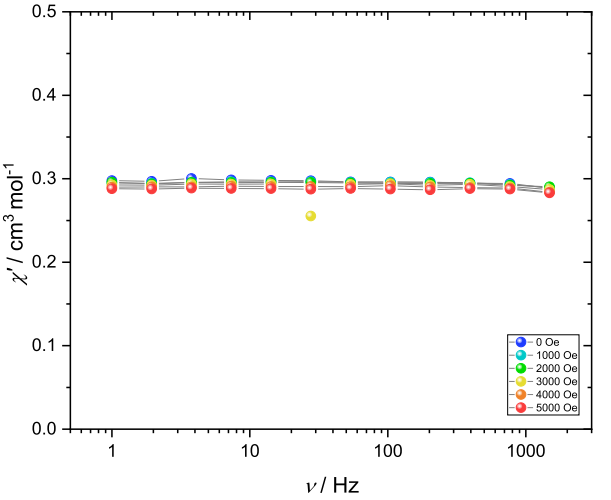


**Supplementary Figure S45.** Field dependence of the in-phase signal of the ac magnetic susceptibility of **TmL**[18]. Solid lines are guidelines for the eye.

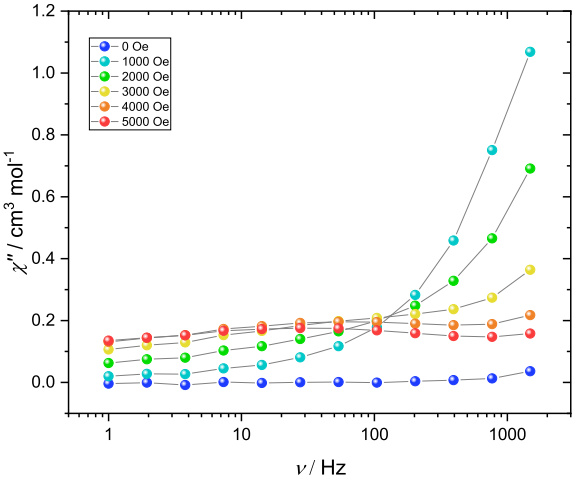


**Supplementary Figure S44.** Field dependence of the out-of-phase signal of the ac magnetic susceptibility of **ErL**[18]. Solid lines are guidelines for the eye.

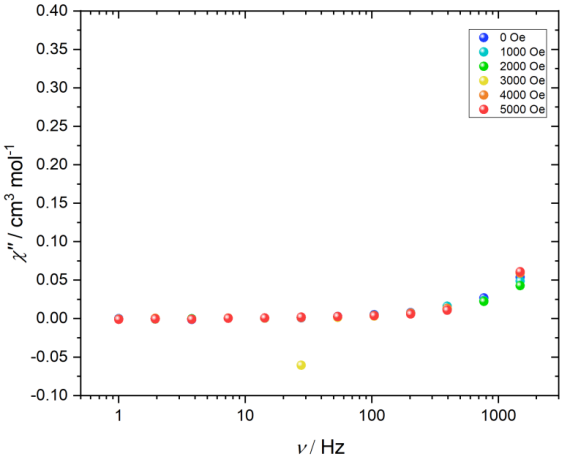


**Supplementary Figure S46.** Field dependence of the out-of-phase signal of the ac magnetic susceptibility of **TmL**[18].

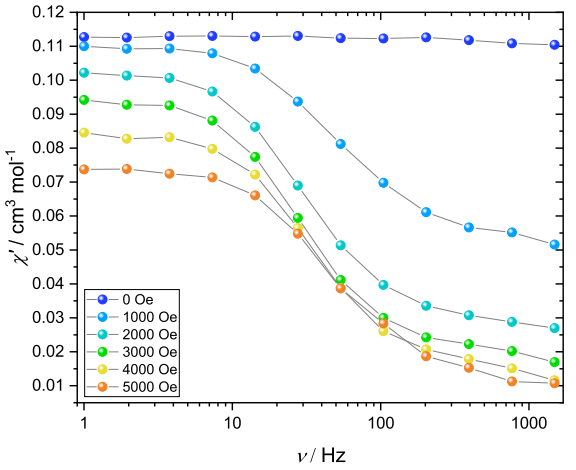


**Supplementary Figure S47.** Field dependence of the in-phase signal of the ac magnetic susceptibility of **Gd@YL$^{18}$** at 5% dilution. Solid lines are guidelines for the eye.

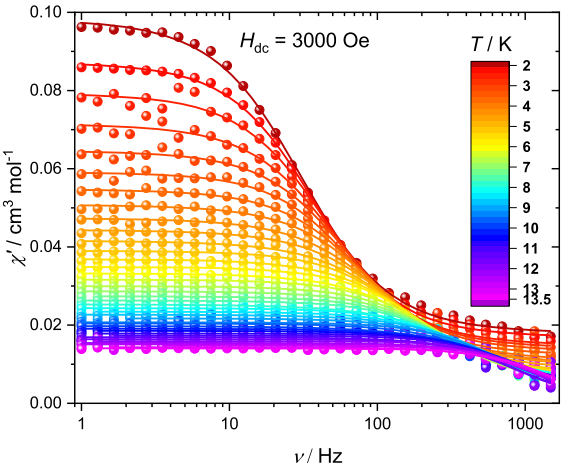


**Supplementary Figure S49.** Temperature dependence of the in-phase signal of the ac susceptibility of **Gd@YL$^{18}$** at 5% dilution. Solid lines are best fits to the generalized Debye model as described in the main text. Parameters can be found in Table S5.

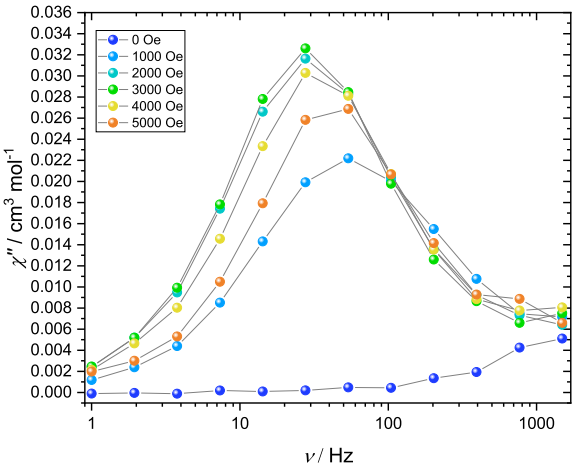


**Supplementary Figure S48.** Field dependence of the out-of-phase signal of the ac magnetic susceptibility of **Gd@YL$^{18}$** at 5% dilution. Solid lines are guidelines for the eye.

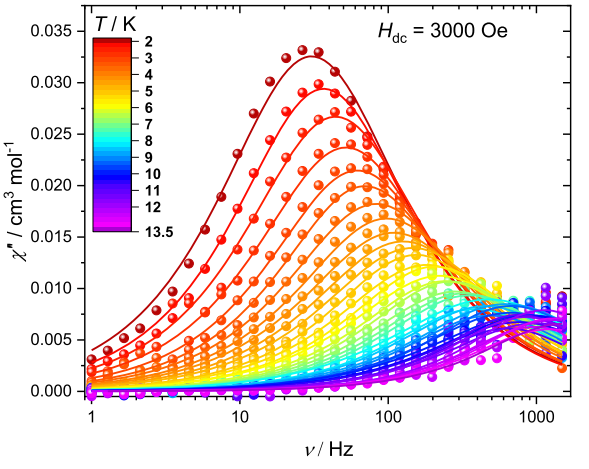


**Supplementary Figure S50.** Temperature dependence of the out-of-phase signal of the ac susceptibility of **Gd@YL$^{18}$** at 5% dilution. Solid lines are best fits to the generalized Debye model as described in the main text. Parameters can be found in Table S5.

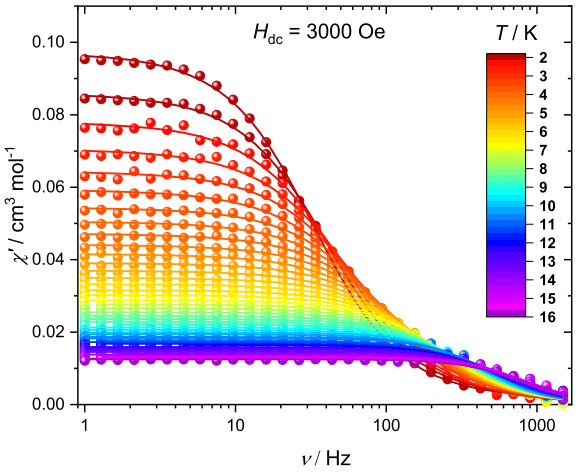


**Supplementary Figure S51.** Temperature dependence of the in-phase signal of the ac susceptibility of **Gd@YL** at 5% dilution. Solid lines are best fits to the generalized Debye model as described in the main text. Parameters can be found in Table S6.

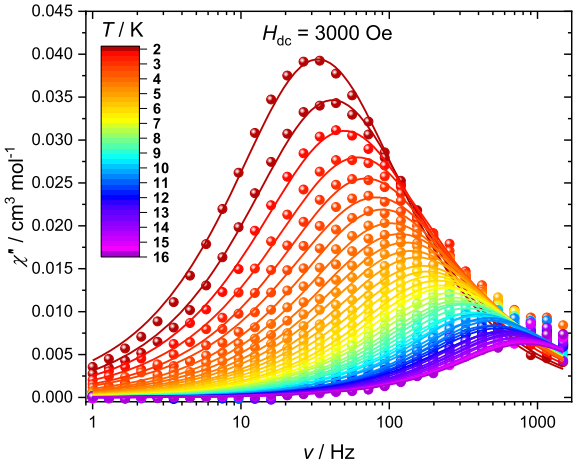


**Supplementary Figure S52.** Temperature dependence of the out-of-phase signal of the ac susceptibility of **Gd@YL** at 5% dilution. Solid lines are best fits to the generalized Debye model as described in the main text. Parameters can be found in Table S6.

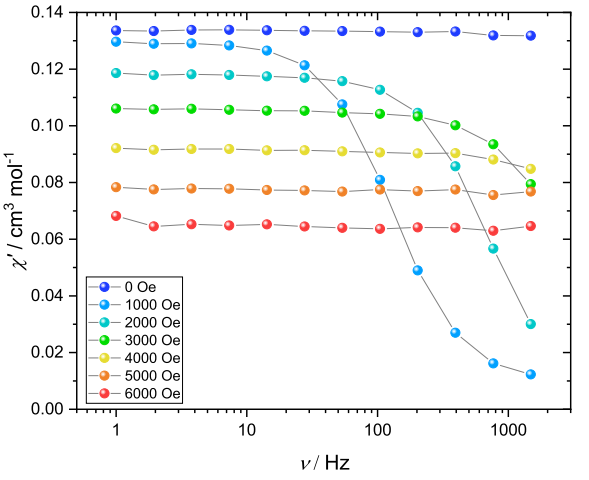


**Supplementary Figure S53.** Field dependence of the in-phase signal of the ac magnetic susceptibility of **Dy@YL**[18] at 5% dilution. Solid lines are guidelines for the eye.

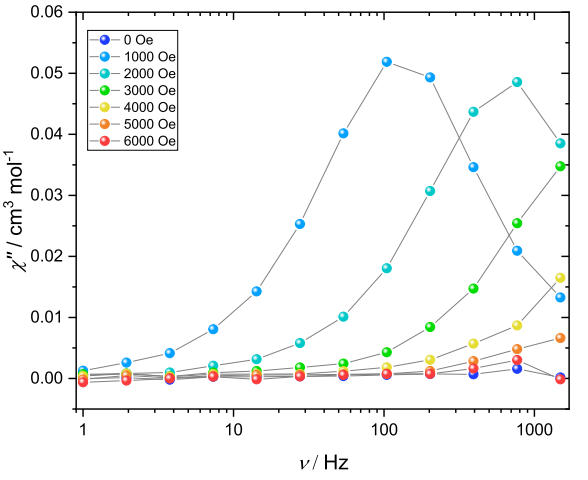


**Supplementary Figure S54.** Field dependence of the out-of-phase signal of the ac magnetic susceptibility of **Dy@YL**[18] at 5% dilution. Solid lines are guidelines for the eye.

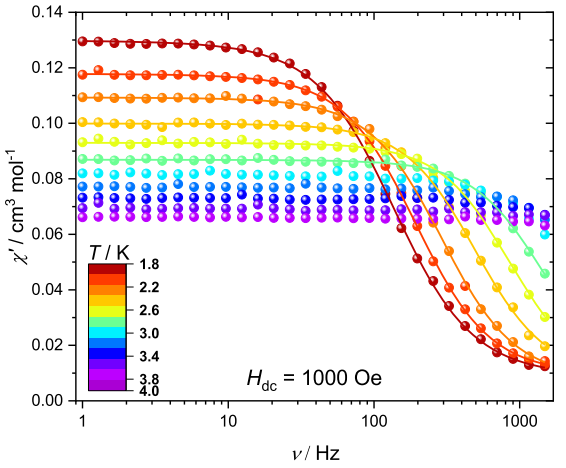


**Supplementary Figure S55.** Temperature dependence of the in-phase signal of the ac susceptibility of **Dy@YL**[18] at 5% dilution. Solid lines are best fits to the generalized Debye model as described in the main text. Parameters can be found in Table S7.

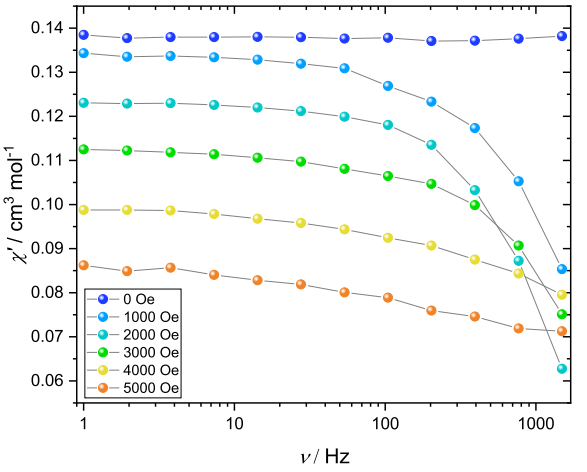


**Supplementary Figure S57.** Field dependence of the in-phase signal of the ac magnetic susceptibility of **Dy@YL** at 5% dilution. Solid lines are guidelines for the eye.

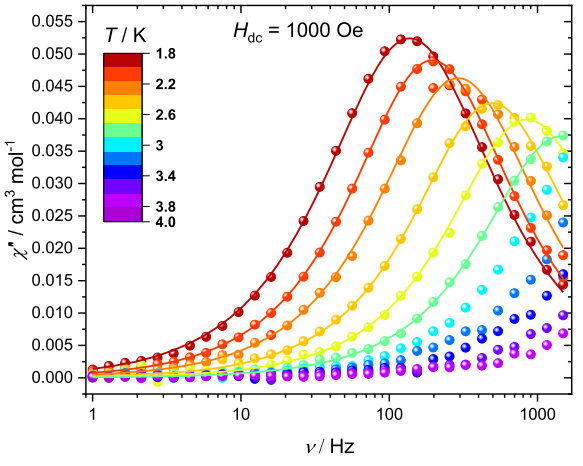


**Supplementary Figure S56.** Temperature dependence of the out-of-phase signal of the ac susceptibility of **Dy@YL**[18] at 5% dilution. Solid lines are best fits to the generalized Debye model as described in the main text. Parameters can be found in Table S7.

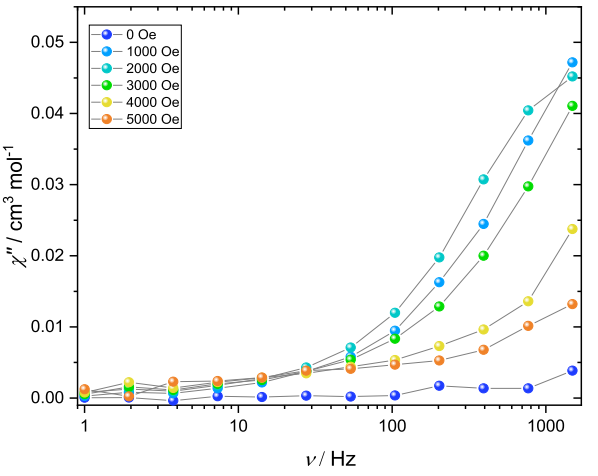


**Supplementary Figure S58.** Field dependence of the out-of-phase signal of the ac magnetic susceptibility of **Dy@YL** at 5% dilution. Solid lines are guidelines for the eye.

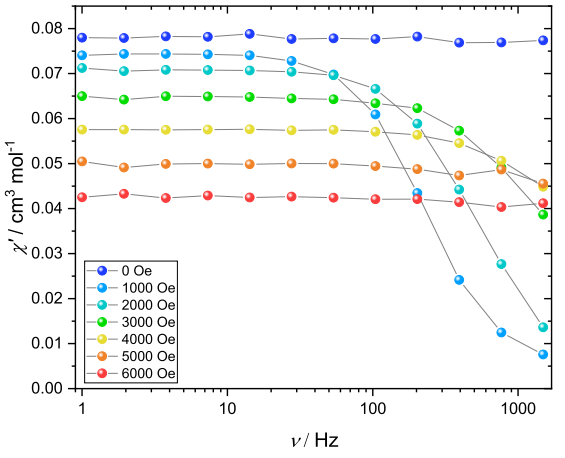


**Supplementary Figure S59.** Field dependence of the in-phase signal of the ac magnetic susceptibility of **Er@LuL$^{18}$** at 5% dilution. Solid lines are guidelines for the eye.

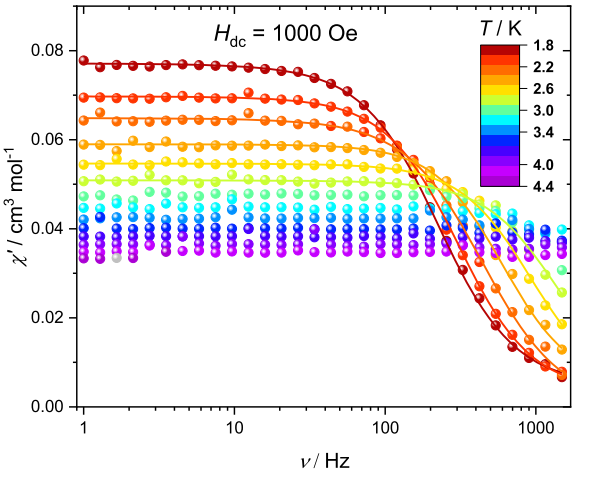


**Supplementary Figure S61.** Temperature dependence of the in-phase signal of the ac susceptibility of **Er@LuL$^{18}$** at 5% dilution. Solid lines are best fits to the generalized Debye model as described in the main text. Parameters can be found in Table S8.

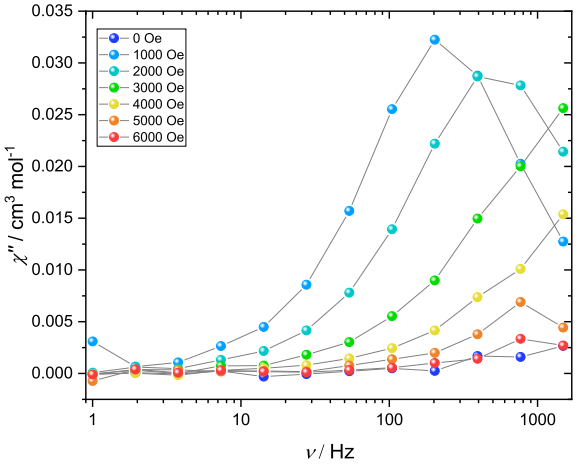


**Supplementary Figure S60.** Field dependence of the out-of-phase signal of the ac magnetic susceptibility of **Er@LuL$^{18}$** at 5% dilution. Solid lines are guidelines for the eye.

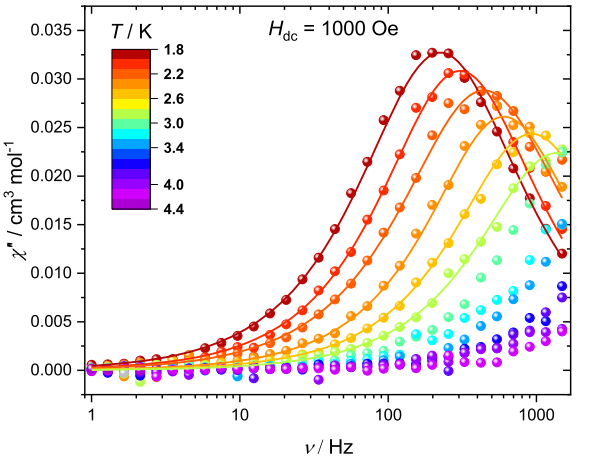


**Supplementary Figure S62.** Temperature dependence of the out-of-phase signal of the ac susceptibility of **Er@LuL$^{18}$** at 5% dilution. Solid lines are best fits to the generalized Debye model as described in the main text. Parameters can be found in Table S8.

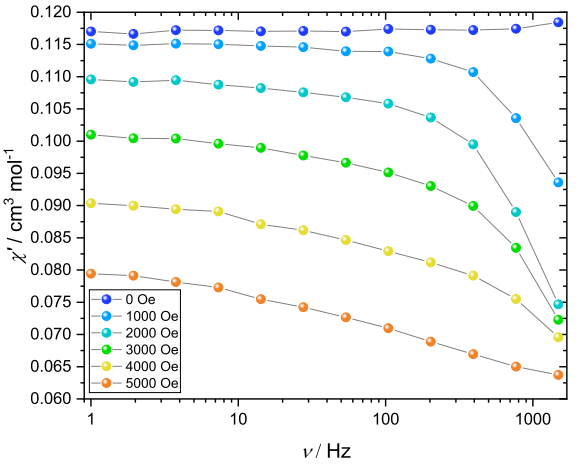


**Supplementary Figure S63.** Field dependence of the in-phase signal of the ac magnetic susceptibility of **Er@LuL** at 5% dilution. Solid lines are guidelines for the eye.

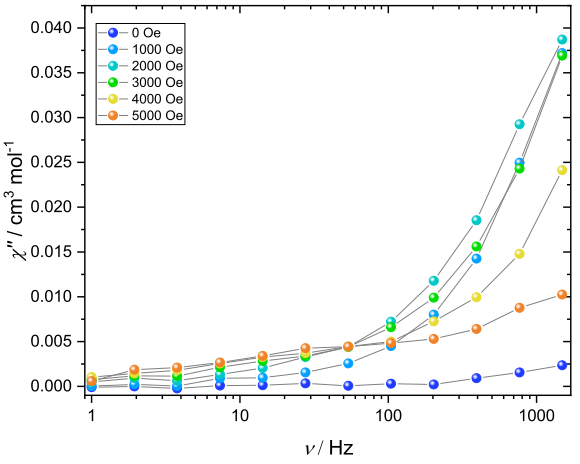


**Supplementary Figure S64.** Field dependence of the out-of-phase signal of the ac magnetic susceptibility of **Er@LuL** at 5% dilution. Solid lines are guidelines for the eye.

**Supplementary Table S5.** Best fit parameters ($\alpha$ and $\tau$) for the generalized Debye model fitted to the temperature dependence of the ac magnetic susceptibility of **Gd@YL**[18] at 5% dilution under an applied magnetic field of 3000 Oe

| $T$ (K) | $\tau$ (s) | $\tau_{error}$ (s) | $\alpha$ | $\alpha_{error}$ |
|---|---|---|---|---|
| 1.8 | 0.005227 | 0.000128 | 0.134341 | 0.013077 |
| 2.1 | 0.004334 | 0.000085 | 0.114181 | 0.010804 |
| 2.4 | 0.003607 | 0.000118 | 0.121189 | 0.017908 |
| 2.7 | 0.003068 | 0.000079 | 0.122059 | 0.014035 |
| 3.0 | 0.002573 | 0.000067 | 0.113528 | 0.014387 |
| 3.3 | 0.002273 | 0.000046 | 0.101008 | 0.011406 |
| 3.6 | 0.001914 | 0.000033 | 0.117228 | 0.009571 |
| 3.9 | 0.001630 | 0.000038 | 0.121731 | 0.012700 |
| 4.2 | 0.001461 | 0.000042 | 0.129688 | 0.015290 |
| 4.5 | 0.001264 | 0.000035 | 0.130148 | 0.014858 |
| 4.8 | 0.001094 | 0.000029 | 0.134491 | 0.013977 |
| 5.1 | 0.001032 | 0.000023 | 0.100714 | 0.012300 |
| 5.4 | 0.000879 | 0.000021 | 0.122918 | 0.012291 |
| 5.7 | 0.000770 | 0.000020 | 0.108410 | 0.013860 |
| 6.0 | 0.000712 | 0.000029 | 0.129031 | 0.021155 |
| 6.3 | 0.000654 | 0.000021 | 0.105658 | 0.016685 |
| 6.6 | 0.000599 | 0.000024 | 0.093375 | 0.021584 |
| 6.9 | 0.000556 | 0.000015 | 0.106179 | 0.014156 |
| 7.2 | 0.000487 | 0.000018 | 0.110416 | 0.019136 |
| 7.5 | 0.000446 | 0.000017 | 0.106190 | 0.019080 |
| 7.8 | 0.000335 | 0.000018 | 0.167977 | 0.021590 |
| 8.1 | 0.000413 | 0.000018 | 0.090410 | 0.022214 |
| 8.4 | 0.000351 | 0.000013 | 0.101395 | 0.017639 |
| 8.7 | 0.000255 | 0.000014 | 0.136898 | 0.020942 |
| 9.0 | 0.000325 | 0.000018 | 0.085032 | 0.028427 |
| 9.3 | 0.000235 | 0.000012 | 0.079646 | 0.023157 |
| 9.6 | 0.000236 | 0.000018 | 0.127383 | 0.030472 |
| 9.9 | 0.000181 | 0.000023 | 0.178832 | 0.039608 |
| 10.2 | 0.000174 | 0.000017 | 0.145751 | 0.031604 |
| 10.5 | 0.000207 | 0.000021 | 0.110499 | 0.038875 |
| 10.8 | 0.000249 | 0.000017 | 0.027080 | 0.035134 |
| 11.1 | 0.000209 | 0.000015 | 0.014138 | 0.035803 |
| 11.4 | 0.000163 | 0.000023 | 0.108758 | 0.050399 |
| 11.7 | 0.000190 | 0.000023 | 0.027219 | 0.056890 |
| 12.0 | 0.000143 | 0.000022 | 0.003018 | 0.064841 |
| 12.3 | 0.000122 | 0.000019 | 0.068331 | 0.050857 |
| 12.6 | 0.000166 | 0.000012 | 0.000000 | 0.032538 |
| 12.9 | 0.000122 | 0.000021 | 0.023942 | 0.063841 |
| 13.2 | 0.000131 | 0.000017 | 0.048305 | 0.045644 |
| 13.5 | 0.000108 | 0.000021 | 0.044593 | 0.063216 |

**Supplementary Table S6.** Best fit parameters ($\alpha$ and $\tau$) for the generalized Debye model fitted to the temperature dependence of the ac magnetic susceptibility of **Gd@YL** at 5% dilution under an applied magnetic field of 3000 Oe

| $T$ (K) | $\tau$ (s) | $\tau_{error}$ (s) | $\alpha$ | $\alpha_{error}$ |
|---|---|---|---|---|
| 1.8 | 0.004815 | 0.000045 | 0.124620 | 0.005097 |
| 2.1 | 0.003831 | 0.000034 | 0.126408 | 0.004810 |
| 2.4 | 0.003186 | 0.000045 | 0.138025 | 0.007509 |
| 2.7 | 0.002597 | 0.000046 | 0.146277 | 0.009220 |
| 3.0 | 0.002278 | 0.000037 | 0.138048 | 0.008652 |
| 3.3 | 0.001959 | 0.000038 | 0.151994 | 0.009921 |
| 3.6 | 0.001766 | 0.000023 | 0.128422 | 0.006865 |
| 3.9 | 0.001562 | 0.000023 | 0.128968 | 0.007803 |
| 4.2 | 0.001357 | 0.000031 | 0.135440 | 0.011863 |
| 4.5 | 0.001238 | 0.000022 | 0.126857 | 0.009546 |
| 4.8 | 0.001146 | 0.000018 | 0.124448 | 0.008497 |
| 5.1 | 0.001039 | 0.000021 | 0.113908 | 0.010815 |
| 5.4 | 0.000960 | 0.000018 | 0.118915 | 0.010030 |
| 5.7 | 0.000887 | 0.000014 | 0.111129 | 0.008546 |
| 6.0 | 0.000822 | 0.000015 | 0.102367 | 0.010128 |
| 6.3 | 0.000754 | 0.000013 | 0.094104 | 0.009293 |
| 6.6 | 0.000713 | 0.000013 | 0.093503 | 0.009889 |
| 6.9 | 0.000669 | 0.000011 | 0.076942 | 0.009589 |
| 7.2 | 0.000614 | 0.000012 | 0.082306 | 0.010432 |
| 7.5 | 0.000586 | 0.000012 | 0.085044 | 0.011270 |
| 7.8 | 0.000552 | 0.000008 | 0.074697 | 0.007650 |
| 8.1 | 0.000523 | 0.000011 | 0.070609 | 0.012061 |
| 8.4 | 0.000496 | 0.000011 | 0.053990 | 0.012054 |
| 8.7 | 0.000471 | 0.000008 | 0.060475 | 0.009431 |
| 9.0 | 0.000455 | 0.000012 | 0.064715 | 0.014234 |
| 9.3 | 0.000419 | 0.000010 | 0.045510 | 0.013156 |
| 9.6 | 0.000403 | 0.000012 | 0.054084 | 0.016414 |
| 9.9 | 0.000388 | 0.000011 | 0.014342 | 0.017188 |
| 10.2 | 0.000361 | 0.000010 | 0.046284 | 0.015812 |
| 10.5 | 0.000339 | 0.000011 | 0.003756 | 0.019990 |
| 10.8 | 0.000317 | 0.000009 | 0.011694 | 0.016977 |
| 11.1 | 0.000324 | 0.000008 | 0.033912 | 0.013699 |
| 11.4 | 0.000305 | 0.000009 | 0.024366 | 0.015700 |
| 11.7 | 0.000294 | 0.000006 | 0.026301 | 0.011842 |
| 12.0 | 0.000270 | 0.000008 | 0.052633 | 0.015504 |
| 12.3 | 0.000274 | 0.000008 | 0.022125 | 0.015146 |
| 12.6 | 0.000265 | 0.000010 | 0.000000 | 0.021648 |
| 12.9 | 0.000245 | 0.000008 | 0.002636 | 0.017164 |
| 13.2 | 0.000235 | 0.000008 | 0.000000 | 0.019727 |
| 13.5 | 0.000233 | 0.000013 | 0.005316 | 0.026853 |
| 13.8 | 0.000224 | 0.000011 | 0.010169 | 0.025218 |
| 14.1 | 0.000215 | 0.000007 | 0.000000 | 0.015904 |
| 14.4 | 0.000198 | 0.000008 | 0.000000 | 0.018189 |
| 14.8 | 0.000205 | 0.000010 | 0.000000 | 0.025022 |
| 15.1 | 0.000194 | 0.000011 | 0.000000 | 0.029080 |
| 15.4 | 0.000200 | 0.000009 | 0.000000 | 0.023481 |
| 15.7 | 0.000192 | 0.000013 | 0.000000 | 0.032827 |

**Supplementary Table S7.** Best fit parameters ($\alpha$ and $\tau$) for the generalized Debye model fitted to the temperature dependence of the ac magnetic susceptibility of **Dy@YL**[18] at 5% dilution under an applied magnetic field of 1000 Oe

| $T$ (K) | $\tau$ (s) | $\tau_{error}$ (s) | $\alpha$ | $\alpha_{error}$ |
|---|---|---|---|---|
| 1.8 | 0.001158 | 0.000006 | 0.092997 | 0.003073 |
| 2.0 | 0.000817 | 0.000003 | 0.064193 | 0.001885 |
| 2.2 | 0.000546 | 0.000004 | 0.059369 | 0.004262 |
| 2.4 | 0.000322 | 0.000003 | 0.046122 | 0.004844 |
| 2.6 | 0.000187 | 0.000003 | 0.045789 | 0.006734 |
| 2.8 | 0.000111 | 0.000002 | 0.043771 | 0.006260 |

**Supplementary Table S8.** Best fit parameters ($\alpha$ and $\tau$) for the generalized Debye model fitted to the temperature dependence of the ac magnetic susceptibility of **Er@LuL**[18] at 5% dilution under an applied magnetic field of 1000 Oe

| $T$ (K) | $\tau$ (s) | $\tau_{error}$ (s) | $\alpha$ | $\alpha_{error}$ |
|---|---|---|---|---|
| 1.8 | 0.000706 | 0.000005 | 0.066960 | 0.004346 |
| 2.0 | 0.000522 | 0.000005 | 0.048358 | 0.005124 |
| 2.2 | 0.000360 | 0.000007 | 0.074909 | 0.009794 |
| 2.4 | 0.000264 | 0.000004 | 0.023578 | 0.008356 |
| 2.6 | 0.000172 | 0.000004 | 0.035732 | 0.008871 |
| 2.8 | 0.000115 | 0.000004 | 0.042868 | 0.012893 |

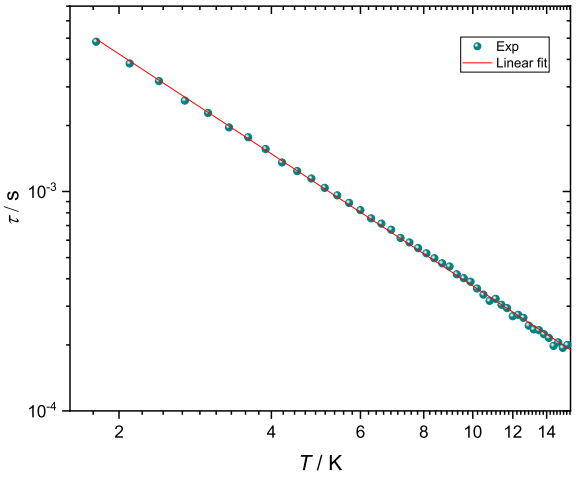


**Supplementary Figure S65.** Relaxation times of **Gd@YL** at 5% dilution as a function of temperature together with the best fit using a direct process as decribed in the main text.

## 7. Luminescence

**Supplementary Table S9.** Electronic transitions ($cm^{-1}$) of **TbL**[18], **TbL**, **HoL**[18], **HoL**, **ErL**[18] and **ErL** obtained from the luminescence spectra presented in the main text

| **TbL**[18] | **TbL** | **HoL**[18] | **HoL** | **ErL**[18] | **ErL** |
|---|---|---|---|---|---|
| 20,492 | 20,500 | 15,423 | 15,442 | 6578 | 6587 |
| 20,354 | 20,358 | 15,385 | 15,399 | 6539 | 6542 |
| 20,109 | 20,105 | 15,333 | 15,356 | 6508 | 6514 |
| 18,471 | 18,484 | 15,211 | 15,230 | 6476 | 6483 |
| 18,420 | 18,430 | 15,029 | 15,042 | 6245 | 6246 |
| 18,298 | 18,308 | 14,975 | 15,002 | | |
| 18,179 | 18,182 | 14,939 | 14,921 | | |
| 18,041 | 18,057 | 14,899 | | | |
| 17,176 | 17,182 | | | | |
| - | 17,117 | | | | |
| 16,838 | 16,846 | | | | |

## 8. UV/Vis spectrum

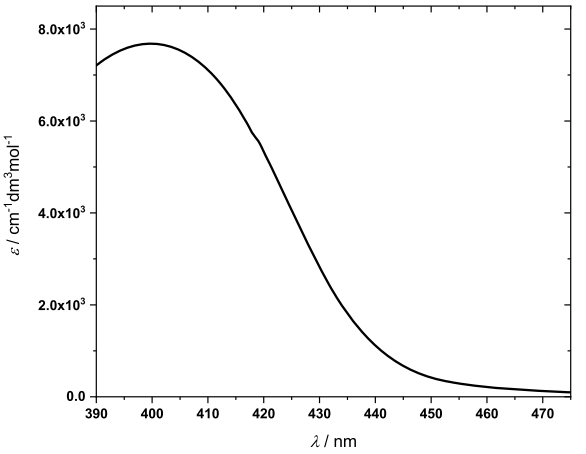


**Supplementary Figure S66.** UV/Vis absorption spectrum of YL[18] in DCM measured at room temperature.

## References

[1] C. D. Buch, S. H. Hansen, C. M. Tram, D. Mitcov, S. Piligkos, *Inorg. Chem.*, 2020, **59**, 16328-16340.